H Y D R O D Y N A M I C F O R C E S
O N
P R O L A T E E L L I P S O I D A L B O D I E S

Thesis by
John Albert Stallkamp

In Partial Fulfillment of the Requirements
for the Degree of
Doctor of Philosophy

California Institute of Technology
Pasadena, California
1954

ACKNOWLEDGMENTS

This writer wishes to thank Professor M. S. Plesset for his advice and assistance in carrying out this program and the Staff of the Hydrodynamics Laboratory for their assistance in the mechanical design and the construction and operation of the equipment.

ABSTRACT

The hydrodynamic forces and moment on submerged bodies of prolate ellipsoidal shape are investigated for two dimensional motion. The specific motion consisted of constant relative linear velocity of the fluid and body and small angular oscillation of the body about its geometric center. The average position of the long axis of the body was in the direction of constant linear motion. The components of the lateral force and of the moment proportional to angular position, velocity, and acceleration are measured for motion in water. These reactions are compared with the reactions derived from perfect fluid theory. It is concluded that the force proportional to angular position is the principal real fluid reaction not predicted by the perfect fluid theory. The deviations of the other components from the theoretical values are small.

TABLE OF CONTENTS

I. INTRODUCTION

For the motion of a rigid body in an infinite volume of incompressible frictionless fluid, the hydrodynamic forces and moments exerted on the body are known at least in principle. Exact analytic solutions are feasible, and often quite easy to acquire, for bodies of simple mathematical shape.

For motion in a real fluid, particularly one whose viscosity is small, it is often possible to use the simpler perfect fluid solution. The accuracy of this approach is evaluated for the lateral force and the moment reactions on a body of prolate ellipsoidal shape.

The perfect fluid reactions are derived for the general two dimensional motion of the ellipsoid in an infinite fluid. The solution includes the case of motion of the fluid at a large distance from the body and is therefore applicable to motion of a test body in a water tunnel.

The experimental procedure and the instrumentation equipment for measurement of the fluid reactions are described. The moment quantities are secured by measurement of the response of the body and fluid system to a sinusoidal torque applied to the body through a spring. The lateral forces are measured directly with a spring balance located in the center portion of the test body.

This force varies sinusoidally with time and is related to the sinusoidal motion of the body.

The experimental results are presented for tests on a series of three prolate ellipsoidal shapes. The tests were made in the High Speed Water Tunnel in the Hydrodynamics Laboratory at the California Institute of Technology.

II. MOTION OF A BODY IN A FRICTIONLESS FLUID

Equations specifying the hydrodynamic force and moment exerted on a rigid body as it moves in an infinite volume of frictionless incompressible fluid are desired. They shall include the forces and moments caused by any motion that the body and fluid or the fluid alone may have. Specifically, they will apply to the motion of a body in a water tunnel in which the fluid has motion independent of the motion of the body.

The several definitions necessary to specify the problem precisely and the appropriate equations of motion of a rigid body in free space will be set forth first. Next the case of motion in large volume of fluid whose motion at an infinite distance from the body is zero will be considered. Finally the motion of a body in a volume of fluid whose motion at a large distance is a non-zero, time-dependent value, will be examined in detail for bodies of a prolate ellipsoidal shape. This last type of fluid motion, constant fluid velocity at a distance, is the one usually assumed in experimental work in a water tunnel in which the tunnel diameter is many times larger than the body diameter.

General Remarks

The two dimensional motion of a prolate ellipsoidal body in a perfect fluid is to be considered in detail.

Some of the derivation will apply to the broader problem of three dimensional motion of an arbitrarily shaped body; this generality, however, will be dropped whenever its continuance would not provide any real information but would only lengthen or complicate the desired derivation. In most instances the extension to include the general case is straightforward.

The rigid body is assumed to be a simply connected volume. Its exterior surface is a smooth impenetrable boundary upon which the surrounding fluid may exert pressure. The resulting force and moment will be shown to be a function of the shape of the body and of the motion of the body and fluid or of the motion of the fluid alone. Experimentally the body will be forced to execute a particular motion and the external force and moment required will give an experimental functional dependence. This dependence will be compared with the perfect fluid dependence to be derived.

The motion takes place in an inertial coordinate system x_o, y_o in which all forces and torques are measured. Angular motion takes place in this plane about an axis normal to it. A second set of axes, x, y, is fixed in the body with origin at the center of mass of the body; These are referred to as body axes. They provide a reference line in the body for the measurement of angular position and define instantaneous directions in the inertial frame along which forces and velocities will

be resolved.

In the experimental work the forces will be measured along body axes and equations for these forces in terms of body motion are desired. These are derived in Appendix I and summarized here.

$$F_x = M(\dot{u} - v\dot{\theta})$$
$$F_y = M(\dot{v} + u\dot{\theta}) \qquad (1)$$
$$N = I_b \ddot{\theta}$$

Note that although the direction of action of the F_x and F_y forces is a function of θ, the magnitude of these forces is measured in the x_o, y_o coordinate system and not in the moving body axes coordinate system.

Motion in a Fluid at Rest at Infinity

This is the classical problem of motion of a body through a fluid. The solution to be given here is from the text of Milne-Thomson.[1] It is given in Appendix II. The several important facts to be observed for this case of motion are given in the following paragraphs.

The motion of the fluid and body may be considered to have started from a state of rest. This defines the inertial system for the subsequent motion. If the body is brought to rest, the fluid motion ceases and all fluid forces and moments become zero.

For finite velocity of the body, the fluid pressure on it is finite and the kinetic energy of the fluid is finite. There is no mechanism for energy loss in the

motion in a perfect fluid. The fluid motion at infinity is zero.

The solution to the problem is a set of parameters that are functions of the shape of the body. They are the coefficients of the velocity terms in the equation of the kinetic energy of the fluid. For a completely unsymmetrical body they are twenty one in number, one for each of the possible quadratic products of the six linear and angular velocities. For a given motion of the body and fluid, the fluid reactions may now be computed from the ordinary $F = Ma$ and $T = I \propto$ equations using the velocities and accelerations of the body.

The solution for the two dimensional motion of a prolate ellipsoid is given in Appendix II. The final equations are

$$\begin{aligned} F_x &= (M + A)\dot{u} - (M + B)\, v\dot{\theta} , \\ F_y &= (M + B)\dot{v} + (M + A)\, u\dot{\theta} , \\ N &= (I_b + R)\ddot{\theta} + (B - A)\, u v . \end{aligned} \tag{2}$$

These equations give the external force and torque on the body required to move it through the fluid with the velocities and accelerations given. The terms containing A, B, and R are the forces and torque that the body exerts on the fluid. Their values for prolate ellipsoids are calculable and will be given in the next part of this section.

Two Dimensional Motion of a Prolate Ellipsoid in a Fluid in Motion at Infinity

For the motion of a body in a water tunnel, a usual assumption of the fluid flow is a constant fluid velocity up and down stream and along the tunnel walls. For the purpose of theoretical analysis the entire space outside this cylindrical working section may be considered to be filled with the fluid moving with this constant tunnel velocity.

In the preceding section the solution for a body moving in a fluid at rest at infinity was formulated. Of particular interest now is the solution for the same relative motion of the body and fluid but with a different absolute flow pattern. Intuitively some of the forces will be the same; they will depend on the relative velocity of the body and fluid only. Perhaps the most obvious one is the static moment represented in Eq. (2) by the term (B - A)uv. On the other hand the behavior of others is not at all obvious. It will be recalled that in the preceding section the problem of motion of a body in a fluid at rest at infinity was solved using that condition explicitly; for example, the kinetic energy in the fluid was finite which required the fluid velocity at infinity to be zero. That part of the solution describing the inertial reactions of the rigid body itself is directly applicable. Particle mass, and therefore

rigid body mass, is an invariant scalar property; the Lagrangian form of the equations of motion contains all of the necessary information. The inertial reactions of the fluid, however, are not of this simple nature unless the motion of each particle of fluid is considered. For the boundary conditions of the preceding section, the integrated effect of the fluid pressures was seen to be representable by inertia type quantities. For the motion of the present section a similar functional dependence on the motion of the body is expected; however, the quantitative measure may be different.

The solution for this general case of motion will be accomplished by integrating the appropriate component of the pressure over the surface of the body. For irrotational motion of a perfect fluid in the absence of an external force field, the pressure equation is

$$\frac{p}{\rho} + \frac{1}{2}\bar{q}^2 - \frac{\partial \phi}{\partial t} = C(t) \qquad (3)$$

The velocity potential ϕ is most easily expressed in terms of the body position and velocity. In this form it moves in space with the body. Its negative gradient correctly expresses the velocity of the fluid in the fixed coordinate system at a given instant of time and may be used to evaluate the $\bar{q}$ term at any point in the fluid. The term $\frac{\partial \phi}{\partial t}$ is required to be the time rate of change of ϕ regarding the point fixed

in space. Now ϕ moves in space with the velocity of the body, $\bar{q}_b$. If $\phi_p(t)$, the potential at a point P fixed in space, is equal to $\phi(t)$ at $t = t_o$,

$$\phi_p(t_o + \delta t) = \phi(t_o) - \int_{t_o}^{t_o + \delta t} (\bar{\nabla} \phi) \, \bar{q}_b \, dt \quad , \qquad (4)$$

and

$$\frac{\partial \phi_p}{\partial t} = \frac{\partial \phi}{\partial t} - \bar{q}_b \, (\bar{\nabla} \phi) \quad . \qquad (5)$$

The pressure equation may now be written as:

$$\frac{p}{\rho} + \frac{1}{2} \bar{q}_r^2 - \frac{\partial \phi}{\partial t} - \frac{1}{2} \bar{q}_b^2 = C(t) \quad , \qquad (6)$$

where

$$\bar{q}_r = \bar{q} - \bar{q}_b \quad , \qquad (7)$$

and ϕ is now the potential referred to the body location in space.

The problem is now reduced to securing this velocity potential for the desired motion of the body, computing the several terms in the equation, and integrating the proper component of the pressure over the surface of the body.

For the two dimensional motion of a prolate ellipsoid the solution is given in Appendix III, The final equations are:

$$
\begin{aligned}
f_x &= -M_o\left[(\dot{u} - \dot{U})\,k_1 - \dot{U} - (v - V)\,k_2\,\dot{\theta} + V\,\dot{\theta}\right] \\
f_y &= -M_o\left[(\dot{v} - \dot{V})\,k_2 - \dot{V} + (u - U)\,k_1\,\dot{\theta} - U\,\dot{\theta}\right] \qquad (8) \\
n &= -I_o\,k'\,\ddot{\theta} - M_o\,(k_2 - k_1)(u - U)(v - V)
\end{aligned}
$$

The definitions of the terms are given in the following list.

f_x, f_y, n	fluid forces and torque on the ellipsoid at and about its geometric center
u, v	velocities of the ellipsoid along body axes
$\dot{\theta}$	angular velocity of the body
U, V	velocities of the fluid at infinity resolved along body axes
k_1, k_2, k'	virtual inertia coefficients for a prolate ellipsoid from Appendix III
M_o	mass of the displaced fluid
I_o	moment of inertia of the displaced fluid

The quantities k_1, k_2, and k' are directly related to the A, B, and R quantities in the preceding section. For U = V = 0, these equations reduce to those of that section.

Examination of the above equations shows that the inertial reactions of the fluid depend only on the relative motion of the fluid and body for the case of constant fluid velocity at infinity. Thus, if U_o and V_o are the components of the constant fluid velocity at a large distance from the body,

$$\begin{aligned} U &= U_o \cos\theta - V_o \sin\theta \ , \\ V &= -U_o \sin\theta + V_o \cos\theta \ , \\ \dot{U} &- V\dot{\theta} = 0 \ , \\ \dot{V} &+ U\dot{\theta} = 0 \ . \end{aligned} \tag{9}$$

If the effects of the finite size of the water tunnel are disregarded, it is seen that, for the same relative velocity of the fluid and body, the perfect fluid forces on a body moving in an infinitely extending volume of fluid at rest at a large distance and the forces on the body moving in a constant velocity water tunnel are identical.

These equations for the fluid forces are now combined with the equations of motion of the rigid body. The complete equations of motion for an ellipsoidal body whose center of mass is at its geometric center are:

$$\begin{aligned} F_x = {} & (M + M_o k_1)\dot{u} - M_o(k_1 + 1)\dot{U} - (M + M_o k_2) v\dot{\theta} \\ & + M_o(k_2 + 1) V\dot{\theta} \ , \end{aligned}$$

$$\begin{aligned} F_y = {} & (M + M_o k_2)\dot{v} - M_o(k_2 + 1)\dot{V} + (M + M_o k_1) u\dot{\theta} \\ & - M_o(k_1 + 1) U\dot{\theta} \ , \end{aligned}$$

$$N = (I_b + I_o k') \dot{\Theta} + M_o (k_2 - k_1)(u - U)(v - V) \quad . \tag{10}$$

In these equations F_x, F_y, and N are external reactions on the body and fluid system.

III. EXPERIMENTAL PROGRAM

Measurements were made to determine the hydrodynamic lateral force and moment on a family of prolate ellipsoidal bodies. The work was done in the High Speed Water Tunnel in the Hydrodynamics Laboratory at the California Institute of Technology.

The scope of the experimental work is discussed first. The experimental method, often referred to as steady state forced oscillation, is described next. The discussion of the calibration and operation of the equipment is divided into several sections. The measurement of the angular motion and moment is given first. After a section describing the construction and general operation of the side force balance, the measurements of the amplitude and phase of the force are discussed separately.

Scope of the Experimental Program

Experimental tests were made to determine the fluid damping and dynamic forces and moment on a series of prolate ellipsoidal bodies for small angle of attack, constant forward velocity motion. In this motion, one point of the body, conveniently taken as the geometrical center for ellipsoids, moves with constant linear velocity. The body is oriented such that its long axis, in

this case the x body axis, is at a small angle from the direction of the constant linear motion. This angle varies with time. The components of the lateral force and moment that depend on the magnitude of this angle are the usual static lift and moment. Other components proportional to the angular velocity and acceleration exist. They are described in the next paragraphs.

In the x_o, y_o coordinate system, the kinematic description of the motion is given by the equations:

$$\begin{aligned} u_o &= u_o = \text{constant}, \\ v_o &= 0 = \text{constant}, \\ \theta &= \theta(t), \\ u &= u_o \cos\theta, \\ v &= -u_o \sin\theta. \end{aligned} \tag{11}$$

Equations (8) for the reaction of the fluid on the body become

$$\begin{aligned} f_x &= -M_o k_1 \dot{u} - M_o k_2 v \dot{\theta} \\ &= M_o (k_1 - k_2) u_o \dot{\theta} \sin\theta, \\ f_y &= -M_o k_2 \dot{v} + M_o k_1 u \dot{\theta} \\ &= M_o (k_2 - k_1) u_o \dot{\theta} \cos\theta, \\ n &= -I_o k' \ddot{\theta} - M_o (k_2 - k_1) u v \\ &= -I_o k' \ddot{\theta} + M_o (k_2 - k_1) u_o^2 \cos\theta \sin\theta. \end{aligned} \tag{12}$$

For the magnitude of θ small, these reduce to

$$f_x = M_o (k_1 - k_2) u_o \dot{\theta} \theta,$$

$$f_y = M_o (k_2 - k_1) u_o \dot{\theta} \quad , \tag{13}$$

$$n = - I_o k' \ddot{\theta} + M_o (k_2 - k_1) \theta \quad .$$

These equations represent perfect fluid reactions only. For this particular motion of the ellipsoid the lateral or lift force is proportional to angular velocity; neither a static nor an acceleration lift force exists. The moment equation exhibits torques proportional to angular position and acceleration, but none to angular velocity. For small angle, the f_x force is of second order compared with the f_y force.

For motion in a real fluid additional fluid reactions are to be expected; for example, a static lift force. No assumptions about the mechanism of these fluid forces are made here. For this motion it is assumed that the lateral force and moment reactions of a real fluid on the body are linear functions of the angular position, velocity, and acceleration of the body. These assumptions are analytically defined by the equations:

$$f_y = - m \ddot{\theta} + b \dot{\theta} + \ell \theta \, , \quad n = - I_f \ddot{\theta} - B \dot{\theta} - K \theta \quad . \tag{14}$$

The component of the lateral force represented by the $b \dot{\theta}$ term is often called the damping force due to angular velocity. The $B \dot{\theta}$ term in the moment equation is called the damping moment due to angular velocity. The six quantities, m, b, ℓ, I_f, B, and K are expected to be

functions of the dimensions of the body, the density of the fluid, and the constant linear velocity of the motion. They are to be determined experimentally. Comparison with their perfect fluid counterparts will give a measure of the effect of the viscosity of the real fluid.

Experimental Method

For the small angle of attack, constant forward velocity motion defined in the preceding section, the measurements of the fluid reactions may be carried out in a water tunnel. The constant forward linear velocity, u_o, of the body is replaced with a constant velocity, $U_o = -u_o$, of the fluid at a distance from the body. The geometric center of the ellipsoid is now fixed in space in the water tunnel. The perfect fluid reactions on the body are not altered by this change in the absolute flow pattern.

For the angular motion it is desirable to choose a steady state, small amplitude, sinusoidal angular oscillation. Although the resulting torque and force have this same sinusoidal time varying character, their measurement can be readily accomplished. An important feature of this steady state type of motion is its averaging property. The motion of a perfect fluid is completely definable from point to point in space and in

time. Real fluid motion does not possess this exact description. Superimposed on any motion is a greater or lesser amount of "noise" or turbulent motion. The integrating property of the steady state method allows the slowly changing components of the fluid reaction to be measured in the presence of more rapidly varying transient effects that would make instantaneous measurement virtually impossible to interpret.

The equations for the total external force and moment on the body may now be written. In the tunnel the geometric center of the ellipsoidal body is fixed in space; its only motion is rotation about this point. This rotation is described by the equation:

$$\theta = \theta_o \sin \omega t \quad , \quad \dot{\theta} = \omega \theta_o \cos \omega t \quad . \tag{15}$$

The center of mass of the ellipsoidal test body is assumed to be located at its geometric center. In the experimental program this was verified; the side force on the bodies when oscillated in air was negligible compared with this force in water. The equations of motion for the rigid body alone reduce to

$$\begin{aligned} F_y &= 0 \ , \\ N &= I_b \ddot{\theta} = - I_b \omega^2 \theta_o \sin \omega t \quad . \end{aligned} \tag{16}$$

The fluid reactions are combined with these to give the total external force and moment on the body and fluid system. The resulting equations are

$$F_y = 0 - f_y = m\ddot{\theta} - b\dot{\theta} - \ell\theta \,, \qquad (17)$$
$$N = I_b\ddot{\theta} - n = (I_b + I_f)\ddot{\theta} + B\dot{\theta} + K\theta \,.$$

These are the external reactions supplied by the supporting structure and measured in the experimental work.

Measurement of Moment

Pictures of the balance installed in the High Speed Water Tunnel are given on pages 89 to 91. A schematic diagram of its operation is given in Fig. 1. The model is secured to a spindle carried in ball bearings in the balance structure. The balance is fastened to the water tunnel underneath the working section.

An ac series motor drives an auxiliary shaft at a constant speed. Velocity feedback speed control is used; the output of a dc tachometer generator, not shown in the schematic diagram, is amplified and excites the control winding of a saturable reactor. This auxiliary shaft also carries a flywheel, the main drive cam, a cam for controlling the time of flashing of a stroboscopic lamp, and an ac tachometer generator.

The drive cam and its follower convert the constant speed rotational motion of the auxiliary shaft into constant frequency, constant amplitude oscillatory motion at the drive platform. This motion is

transferred through a torsion drive spring to the spindle and then to the model. The diameter of a short section of the upper part of the spindle is small enough so that it acts like a second torsion spring.

In Eq. (17) the body and fluid are shown to be equivalent to a moment of inertia, an angular damping rate, and an angular spring rate. The equivalent mechanical diagram for the angular motion is given in Fig. 2. The several quantities are defined in the following list.

I, B, and K	moment of inertia, angular damping rate, and angular spring rate for the body and fluid system
K_1, K_2	main drive spring rate, upper spring rate
I_s	moment of inertia of spindle
B_s	angular damping rate of seal
θ, θ_1, θ_2	motion of model, spindle, drive platform

The seal between the spindle and the wall of the water tunnel consists of a thin cylindrical space of approximately .001 inch radial clearance on a .875 inch diameter and of one inch length. For the tunnel pressures used, the rate of water leakage was about ten gallons per hour; this water was collected by a vacuum system before it reached the spindle bearings

and was discarded. The damping rate of this seal is smaller than can be measured in the operation of the balance. The moment of inertia of the spindle is small but not negligible at all times. These two items are discussed in Appendix IV.

The solution for steady state oscillatory motion is now formulated. The damping rate of the seal is not included.

$$\begin{aligned} \theta_2 &= A_2 \sin(\omega t - \alpha_2) && \text{drive motion} \\ \theta_1 &= A_1 \sin(\omega t - \alpha_1) && \text{spindle motion} \\ \theta &= A_o \sin(\omega t - \alpha_o) && \text{model motion} \end{aligned} \tag{18}$$

The angles α_o, α_1, and α_2 are angles of lag in the time sense. The differential equations of motion of the system are

$$\begin{aligned} K_1(\theta_2 - \theta_1) - K_2(\theta_1 - \theta) &= I_s \ddot{\theta}_1 , \\ K_2(\theta_1 - \theta) &= I\ddot{\theta} + B\dot{\theta} + K\theta . \end{aligned} \tag{19}$$

In the complex variable form used in steady state alternating current problems, the steady state solution is given in the following equations.

$$\left\{\frac{K + K_2}{K_2} - \frac{I\omega^2}{K_2} + \frac{j\omega B}{K_2}\right\}^{-1} = \frac{K_2 + K_1}{K_2} - \frac{I_s\omega^2}{K_2} - \tag{20}$$

$$\frac{K_1 A_2}{K_2 A_1}\left\{\cos(\alpha_2 - \alpha_1) - j\sin(\alpha_2 - \alpha_1)\right\}$$

$$\frac{A_o}{A_2}\left\{\cos(\alpha_2 - \alpha_o) + j\sin(\alpha_2 - \alpha_o)\right\} = -\frac{I_s\omega^2}{K_2} + \frac{K_2 + K_1}{K_2}\frac{A_1}{A_2}\left\{\cos(\alpha_2 - \alpha_1) + j\sin(\alpha_2 - \alpha_1)\right\} - \frac{K_1}{K_2} \quad (21)$$

Examination of these equations shows that the data necessary to compute the I, B, and K quantities for the model and fluid system are the frequency of oscillation and the amplitude ratio and relative phase angle of the drive platform and spindle motions. Measurements must be taken at two or more frequencies to separate the I and K terms.

The oscillation frequency was continuously monitored with an electronic counter* that measured the period of the output voltage of the ac tachometer generator. An extremely constant frequency was desired to facilitate the measurement of side force to be described in the next section. Speed stability of better than .05 percent was achieved over the range of four to ten cps with the saturable reactor equipment. At two cps, the lowest frequency used, the stability was about .1 percent.

The amplitude ratio and phase relationship was measured stroboscopically. Electrical contacts, actuated by a cam on the auxiliary shaft, were mounted on a

---

* Hewlett-Packard Co., Palo Alto, Calif., Model 522B

circular carriage concentric with this shaft. The angular location of these contacts determined the time in the cycle of motion of the flashing of a General Electric type FT-110 flash tube. The short duration flash of light was passed through a slit and directed at mirror and lens combinations mounted on the drive platform and the spindle. Each of these mirror and lens units reflected and focused the light on a curved screen about six feet away. The cam had two actuating surfaces spaced 180 degrees apart. For each revolution two flashes of light occurred. These were spaced 180 degrees apart in the cycle of the oscillatory motion; for example at zero and 180 degrees. For the same position of the contact carriage, a second set of two flashes, located at relative positions of 90 and 270 degrees, was available.

In typical operation, twenty four point wave forms of the steady state drive motion and response motion are taken. This is done by moving the contact carriage in 15 degree increments. The amplitude and phase angle of the fundamental component of each motion is then determined by Fourier analysis. In an alternate method the contact carriage is rotated until the two flashes of light occurring for each revolution coincide on the scale. This is the mid-point of the oscillatory motion and can be taken as a measure of the phase angle. The

amplitude of the motion is then measured by selecting the other set of two flashes that are spaced 90 degrees from these. The former method was used in all cases for the measurement of the response motion. In the presence of transients it was easier and more accurate to read the average position of a single recurring light flash than to try to estimate the degree of coincidence of two alternatingly recurring flashes. The drive motion contained less than 1 percent total harmonic distortion most of which was second harmonic. For the water tunnel velocities and oscillation frequencies used, the harmonic content of the response motion was less than 2 percent.

A picture of the control rack for the angular measurement equipment is given on page 92. The black box on top of the rack contains the saturable reactor and control equipment for the main drive. The bottom panel unit in the rack is the dc amplifier in the feedback loop of the speed control system. The top panel contains the controls for moving the contact carriage and selecting the contact combinations. The larger panel directly below this contains the hydrogen thyratron modulator unit for flashing the lamp. Behind and slightly to the left of the top box, the scale can be seen. The grey box with the air hose connection contains the lamp. Both the scale and the lamp box are rigidly fastened to the tunnel structure. The view

is downstream.

The measurement of the amplitude ratio and the relative phase angle for the wave form analysis method is accurate to the order of .5 percent. This figure applies to the capability of the instrumentation method and equipment. The accuracy of measurement of the hydrodynamic reactions is discussed in the next part in which the numerical results of the experimental work are given. The smallest division on the scale and the width of the light image was equal to about .01 degree of rotation at the spindle. All of the measurements were made at frequencies well below the natural frequency of the system; the half amplitude of the drive motion was 2 degrees, and the maximum half amplitude of the model motion was less than 3 degrees. The accuracies of the 15 degree increments of contact carriage rotation, the 180 degree spacing of the flats on the cam, and the 90 degree spacing of the two sets of light flashes are all better than .1 degree. This is equivalent to less than .1 percent error in amplitude. These accuracies were determined by stroboscopic techniques. The primary standard of angular measure was a set of marks on the perimeter of the 18 inch diameter flywheel; these marks had been located with a precision dividing head.

Measurement of Lateral Force

The lateral force on the body was measured by a spring balance structure located inside the center portion of the body. Figure 3 is a diagram of the essential features. This balance section was used for the three models; the aluminum ellipsoidal shells fitted over it.

The outer shell of the balance structure proper was fastened to the spindle by means of a parallelogram flexure linkage. The moment reaction was transmitted as tension and compression in the parallel links. The lateral force between the body and spindle was carried in a stiff open-coil spring. The small cross section of the flexure links permitted motion in the lateral direction. The natural frequency of this degree of freedom, based on 3000 lb per in spring constant and less than one lb mass, is greater than 160 cps. For oscillation frequencies of 10 cps or less, the lateral motion is spring controlled; and the instantaneous lateral deflection is a measure of the lateral force at that instant. For the maximum force of 3 lb this deflection is about .001 inch; the fluid reaction of this motion is negligibly small compared to that of the angular motion.

The electrical connection to the pickup unit was made through the spindle. The interior of the balance

section was filled with air and pressurized to about 2 psi above the dynamic fluid pressure of the water tunnel. This differential was maintained by an ordinary pressure regulator. By using the dynamic tunnel pressure for the reference or pilot pressure of the regulator, the pressure level of the tunnel could be changed without producing an excessive pressure difference across the thin rubber diaphragm between the spindle and the shell of the balance. Dried air was used. While data was not actually being taken, air was passed through a relief valve into the tunnel to keep the interior of the balance free from any moisture.

The assumed functional form of the side force for motion in a real fluid was presented in Eq. (17). In the complex notation for steady state sinusoidal motion this equation becomes

$$F_y = 1.414\, F_i \sin(\omega t - \alpha_i) = -(m\omega^2 + \ell + j\omega b) A_o \sin(\omega t - \alpha_o) , \tag{22}$$

and,

$$m\omega^2 + \ell + j\omega b = -\frac{\sqrt{2}\, F_i}{A_o}\left\{\cos(\alpha_o - \alpha_i) - j \sin(\alpha_o - \alpha_i)\right\}. \tag{23}$$

The determination of m, b, and ℓ requires the measurement of the magnitude and phase angle of the sinusoidally varying side force.

A linear differential transformer* was used as the transducer element. The electrical output of this device is proportional to the relative linear position of its center iron slug and the concentric winding structure. It was mounted in the center section as shown in Fig. 3. A carrier frequency of 1000 cps was used. The output voltage was an amplitude modulated wave. The center position of the slug was set far enough from the electrical null of the pickup so that the degree of modulation was less than 100 percent for the maximum side force experienced.

A block diagram of the electronic equipment is given in Fig. 4. The peak output of the pickup unit is on the order of millivolts for the typical force on the body. It is first amplified 40 db in a conventional feedback amplifier. It is passed through an L-C filter, whose narrow pass band is centered at the 1000 cps carrier frequency, to remove unwanted noise components. After another 40 db amplification, it is demodulated in a bridge crystal rectifier unit to recover the modulating signal. A low pass filter removes the undesirable 2000 cps rectified carrier signal. The output of the filter appears across a load resistor. It is a sinusoidal voltage of the frequency of the motion of the model. Its magnitude is proportional to the magnitude

---

* Schaevitz Engineering, Camden, New Jersey, Type 005M

of the side force; its phase is the phase of the side force plus the frequency dependent phase shift of the several intermediate circuits.

The actual measurement of the voltage is accomplished by a null method. The output of the ac tachometer generator is a voltage of the same frequency as the model motion. After isolation by a cathode follower, it is added to the voltage to be measured. The magnitude of the generator voltage is adjustable by attenuators and its phase is adjustable by rotating the frame of the generator itself. The sum of the voltages is passed through a twin-T feedback, narrow pass, amplifier to remove the last remnants of noise voltages and is then presented on the vertical axis of an oscilloscope. When the horizontal axis is driven sinusoidally with one of the voltages, the type and direction of the difference between the voltages is interpretable from the orientation and shape of the elliptical pattern on the oscilloscope. The amplitude data appears in the form of an attenuator setting and the phase data is given by the reading of a mechanical counter geared to the motion of the generator frame.

A picture of the control rack is given on page 93. The top unit is the electronic counter for the measurement of the frequency of motion; the oscilloscope is next. The counter and control for the angular motion

of the frame of the generator are located on the left side of the first black panel. The attenuators for the amplitude measurement are on the right side. The second black panel unit is the two stage twin-T amplifier. The next panel contains the first 40 db amplifier and the 1000 cps filter on the left and the demodulator and 2000 cps filter on the right. The last three units are the second 40 db amplifier, a dc power supply, and the 1000 cps oscillator.

It will be recognized that for the most part the individual electronic circuits and items of equipment are conventional. The application of the twin-T feedback amplifier and the phase shift considerations of the L-C filters are the only items considered to be sufficiently unusual to require further description. The latter will be done in the section describing the measurement of the phase of the lateral force.

The twin-T rejection amplifier consisted of two identical single stage amplifiers. Negative feedback was applied around each stage through an adjustable stop frequency, twin-T resistor-capacitor network. At the rejection frequency of the network, the gain was about 20 db per stage. It dropped rapidly to about 0 db for frequencies beyond one octave above and below this frequency. The two stages in cascade gave about 40 db rejection. The desired pass frequency was

adjustable from one to fifteen cps by means of the three gang helipot in the twin-T network. The narrowness of the pass band and the rapid phase shift through it made extreme speed stability necessary if the rejection property of the amplifier was to be useful in obtaining the null balance. Because the electrical signals to be balanced were already added together before reaching this unit, its absolute gain or phase shift did not affect the measurement. But the interpretation of the type of unbalance from the pattern on the oscilloscope can be accomplished easily for phase shifts of zero or multiples of 90 degrees only. In this case the phase shift was 360 degrees. The tilt or angle of the horizontal axis of the elliptical pattern was a measure of the amplitude unbalance, and the vertical opening or eccentricity of the ellipse was a measure of the phase difference of the two voltages.

1. Amplitude Measurement

It will be convenient to discuss the measurement of the amplitude and phase of the lateral force separately.

The calibration and operation of the amplitude measurement portion of the equipment is carried out on a basis of relative measurements. It is not necessary to determine the value of any electrical quantity in the

absolute sense; precision type dc milliammeters are used not for their quantitative accuracy but for their linearity and the preciseness of their readings.

The 1000 cps carrier voltage input to the pickup unit was measured with a bridge type instrument rectifier and a dc milliammeter. These were permanently connected to the oscillator. Only a relative measure of the voltage was necessary. The slow drift after a short warm up time never exceeded a few percent in a day. The reading of the milliammeter was recorded as an item of data for each measurement of force.

A second precision dc milliammeter was used for calibration of the pickup unit and the amplifiers, filters, and demodulator equipment. It could be plugged into the load resistor circuit. The plugging-in action removed a portion of the load resistor equal to the resistance of the meter. The inductive reactance of the meter coil produced a measurable phase shift; the meter was removed from the circuit during the actual measurement of dynamic forces.

The amplitude equation is now formulated.

All quantities are dc or rms values.

f	cps	frequency
F_i	lb	force
V_o	volt	oscillator voltage

i	ma	increment in dc current in load resistor for static force
g_1		gain setting of resistor divider between amplifiers
g_o		gain factor of amplifiers
s	ma volt^{-1} lb^{-1}	sensitivity, ma in load resistor per input volt per lb for $g_1 = 1$
p	volt ma^{-1}	ratio of voltage across load resistor with milliammeter out to dc ma with meter in
V_r	volt	voltage across load resistor
v	volt cps^{-1}	ac tachometer generator rate constant
h		helipot setting
A_t		attenuator setting

The null condition is represented by the equations:

$$F_i \, s \, g_1 \, g_o \, V_o \, p = V_r = v \, f \, h \frac{1}{A_t} \quad , \tag{24}$$

$$F_i = \frac{v}{p} \frac{1}{s} \frac{1}{g_o} \frac{h \, f}{g_1 \, V_o \, A_t} \quad . \tag{25}$$

The static force equation is

$$F_i = s\ g_1\ g_o\ V_o * i \quad . \tag{26}$$

The five quantities, h, f, g_1, V_o, and A_t, were taken as data for each measurement of dynamic force.

The measurement of the amplifier gain, g_o, was accomplished by connecting a fraction of the oscillator voltage into the first amplifier and measuring the dc current in the load resistor. Four audio output transformers connected in cascade provided the necessary constant fractional reduction in voltage. Since the tests were always made at the same values of g_1 and V_o, the quantity g_o may be represented by the equation:

$$g_o = c_g\ i_g \quad . \tag{27}$$

The constant c_g will be cancelled out in later equations. The gain as measured by the current i_g was observed from time to time during each day. It would vary slowly over a range of a few percent; usually a set of several runs would have the same value of gain. At the same time as these readings were taken, the linearity of the demodulating equipment was observed by changing the fractional gain g_1. The linearity was as good as the meter* which has a linearity of .2 percent.

The sensitivity constant, s, was determined by static dead weight tests on the model. Static horizontal

---

* General Electric Co., Schenectady, N. Y., Type DP-2

forces were applied to the model by wire and pulley arrangements using the force of gravity on mass weights. Five equal increments of force were applied in one direction and then in the other. By this procedure the incremental change in current in the load resistor per unit of force was determined. It will be recalled that this is a carrier system, and that it is the change in rectified carrier output that is a measure of the modulating signal. The procedure is expressed analytically in the following equations. The F_s and i_s are the incremental changes in force and current. The quantity i_g, is the measure of the amplifier gain, g_o , at the time of the measurements.

$$F_s \; s \; g_1 \; g_o \; V_o = i_s \tag{28}$$

$$s = \frac{1}{F_s \, g_1 \, V_o} \; \frac{i_s}{g_o} = \frac{1}{F_s \, g_1 \, V_o} \; \frac{i_s}{c_g \, i_g,} \tag{29}$$

Twenty two sets of measurements were made at more or less regular intervals during the experimental program. Each set represented the average of the values of incremental current for several cycles of increments of force. When the appropriate values of the other quantities are supplied, the following value of the product ($s \; c_g$) is arrived at:

$$(s \; c_g) = .400 \pm 1 \text{ percent.} \tag{30}$$

The quantities v and p are constants of the equipment. It was not necessary to determine their individual values.

Their ratio was measured by using the constant amplitude motion of the drive platform of the moment balance. A second differential transformer picked up this motion, and the resulting electrical signal was measured. By rotating the auxiliary shaft by hand, the static or dc maximum and minimum values of the current in the load resistor were determined. These corresponded to the maximum and minimum positions of the drive platform. The equivalent rms value of current for this case of zero frequency motion was computed. The balance was then run at a series of frequencies and the usual amplitude data were taken. Since the amplitude of the motion is constant, these two cases of motion may be equated. Equations (24) and (26) are used.

$$i_p = V_r = v\, f\, h \frac{1}{A_t} \tag{31}$$

The average value of the $f\, h\, A_t^{-1}$ product in per second units over a range of four to ten cps was 1.64 ± .01. The resulting value of $v\, p^{-1}$ in ma per cps is .0225 ± .0001.

When the numerical values presented in the preceding parapraphs are collected, the final equation for the amplitude of the lateral force is given. Since the value of g_1 was constant in all of the actual runs, its value of one third is put into the equation.

$$F_i = .0225 \frac{1}{.400} 3 \frac{1}{i_g} \frac{f\,h}{V_o\,A_t}$$

$$= .169 \frac{1}{i_g} \frac{f\,h}{V_o\,A_t} \qquad (32)$$

2. Phase Measurement

The measurement of the phase of the lateral force relative to the motion of the body required the tracing of an electrical phase from the pickup unit through the electronic equipment to a mechanical position of the frame of the ac tachometer generator, across a mechanical gap to the location of the contacts for flashing the stroboscopic lamp, and finally to the phase of the angular motion of the body.

The angular location of the contact carriage is a reference for the phase of the angular motion of the body. Its position was measured by a mechanical counter geared to it through a worm and spring-loaded worm wheel and a selsyn repeater circuit. The counter reading for the zero phase of the drive motion is determined from the Fourier analysis of the drive motion wave form. The phase difference between the drive motion and the model motion is calculated by Eq. (21).

The angular location of the ac tachometer generator frame was also measured with a mechanical counter. The phase difference of the drive motion and the voltage generated by tachometer was determined with an oscilloscope. The sine wave voltage was displayed on one axis. The square pulses generated each half cycle by the closing of the contacts were displayed on the other. The frame of the generator was rotated until the leading edges of the two pluses coincided. The generated voltage and the action of the contacts were now considered to be in phase; the readings of the two counters were the data that provided a connection between angular motion phase and side force phase measuring equipment.

Between the differential transformer pickup unit and the demodulator the signal information is carried in the side bands of the modulated wave. The effect of phase shift at the carrier and side band frequencies on the modulating signal is discussed in Appendix V. It is shown that for the steady state condition the signal wave form is not distorted, and its phase shift is a delay proportional to the signal frequency.

The phase shift in the electronic equipment from the side force pickup unit to the load resistor was calibrated with the second pickup using the drive platform motion. This phase data was taken at the same time as the amplitude data for determining the ratio of the quantities v

and p. The measured value of rate of phase shift was 2.17 degrees per cps. The measured value of the rate of phase shift for the 1000 cps L-C filter alone was 2.12 ± .06 degrees per cps. See Appendix V for an analysis of the phase shift through this filter.

The equation for the total phase shift from pickup to drive motion is

$$\alpha_i - \beta\omega = \alpha_{T_i} - (\alpha_T - \alpha_2) . \qquad (33)$$

α_i phase of force

α_2 phase of drive motion

α_{T_i} generator frame counter reading

α_T counter constant, connection between force and angular measurement equipment

β rate of phase shift for force measurement electronic equipment

The equipment was capable of measuring angles of .1 degree. The percentage equivalent of this figure is less than the 1 percent accuracy of the amplitude measurement for phase angles greater than 10 degrees.

IV. EXPERIMENTAL RESULTS

Test Conditions

Experimental tests were made with three prolate ellipsoidal shapes. All of the test bodies were two inches in diameter. The lengths were six, ten, and fourteen inches which represent aspect ratios of 3:1, 5:1, and 7:1. These shells were made of aluminum; the wall sections were made as thin as structurally possible in order to further minimize their moment of inertia. The external surface was polished to about a five micro-inch finish. Dimensional tolerances were held to the order of .001 inch.

The water tunnel velocities ranged from zero to 25 ft per sec in five ft per sec increments. These were nominal values. The velocity was measured for each run, and this value was used to reduce the data of that run.

Frequencies of oscillation of two, four, six, eight, and nine or ten cps were used. The drive platform amplitude for all tests was two degrees. The amplitude of oscillation of the test bodies was a function of the tunnel velocity and the frequency. Its maximum value was less than three degrees for all tests.

The tunnel pressure at the working section was held between five and ten psi gauge. Variations in pressure did not produce any measurable changes in the fluid

reaction on the body. These pressures were high enough to suppress cavitation at all tunnel velocities.

The upper limits of the tunnel velocity and oscillation rate were set by the structure of the internal force balance and the unsteadiness of the motion. The amount of torque that could be transmitted in the flexure links was the limiting factor for the force balance. The second limit, the unsteadiness of the motion, is inherent in motion of a real fluid. There was some transient reaction on the body at the lower tunnel velocities, but there was no difficulty in estimating the average value of a reading. Two observers taking the twenty four point wave form data independently would obtain angular amplitude and phase values that agreed to better than one percent. At 25 ft per sec tunnel velocity the transient disturbances were about 15 to 20 percent of the amplitude of the fundamental frequency.

Data Reduction

The reduction of the data to intermediate curves is presented in this section. The final numerical results are given in the next section.

1. Angular Quantities

The real and imaginary parts of Eq. (20) are separated.

$$\text{Real Part} = \frac{K + K_2}{K_2} - \frac{I\,\omega^2}{K_2} \qquad (34)$$

This quantity is plotted versus the square of frequency, f, in Fig. 5, 6, and 7 for the three bodies. The curves are approximately straight lines for each tunnel velocity. From the intercept and slope of each line a value of K and I is calculated.

$$\text{Imaginary Part} = \frac{\omega\, B}{K_2} \qquad (35)$$

The value for B for a perfect fluid is zero. The experimental value for real fluids is small. For each tunnel velocity an upper limit of its value is determined. Sample calculations for a typical run are given in Appendix VI.

2. Lateral or Side Quantities

The rms value of the side force and the phase angle between it and the drive motion are computed from data using Eq. (32) and (33). The phase angle and amplitude ratio of the angular motions of the drive platform and body are computed from data using Eq. (21).

Equation (23) containing the side force constants m, b, and ℓ is now separated into its real and imaginary parts. The real part is equal to $(m\,\omega^2 + \ell)$. In the

same manner as for the angular quantities, this term is plotted versus the square of frequency. These curves are presented in Fig. 8, 9, and 10. They are not the straight lines that the assumption of components of side force proportional to angle of attack and to angular acceleration predict. The zero frequency intercept is taken as the measure of the static lift force. The slope of the straight portion of the curves is taken as a measure of the side force proportional to angular acceleration. Both of these reactions are zero for perfect fluid motion.

The imaginary part of Eq. (23) is equal to ωb. This quantity is plotted versus frequency in Fig. 11, 12, and 13. This fluid reaction exists in a perfect fluid and is proportional to the frequency of oscillation and the velocity of the tunnel for this motion of the body. The experimental curves are straight lines as predicted by the theory.

Sample calculations for a typical run are given in Appendix VI.

Experimental Results

1. Hydrodynamic Moment on Prolate Ellipsoidal Body

Equation (14) gives the real fluid hydrodynamic moment on the body in terms of three quantities, I_f, B, and K. The experimental values of these are now given. The corresponding values for perfect fluid motion from Eq. (13) are also presented.

a. Static Moment

The dimensionless quantity $(k_2 - k_1)$ is a measure of the static moment rate. Experimental and perfect fluid values are given in Fig. 14. The perfect fluid value is calculated from equations in Appendix III. The quantity K is equal to $M_o U_o^2 (k_2 - k_1)$ where M_o is the mass of the displaced fluid and U_o is the constant relative linear velocity.

b. Moment due to Angular Velocity

The dimensionless quantity c_k is called the damping moment rate. For perfect fluid motion it is zero. For real fluid motion in the range of the experimental tests it is small. Experimental values representing its estimated maximum are given in Fig. 15 for Reynolds number based on the length of the body. The basis of dimensionality is the equation:

$$B = c_k \frac{\rho}{2} U_o A (2a)^2 \quad . \tag{36}$$

The quantity A is the area of the circular cross section of the prolate ellipsoid and (2a) is the length.

c. Virtual Moment of Inertia of Fluid

The dimensionless quantity k' is the coefficient of virtual moment of inertia of the fluid. The experimental and perfect fluid values are given in Fig. 16. The perfect fluid value is calculated from the equation in Appendix III. The quantity I_f is equal to k' I_o where I_o is the moment of inertia of the displaced fluid.

2. Hydrodynamic Lateral Force on Prolate Ellipsoidal Body

Equation (14) gives the real fluid lateral force on the body in terms of the quantities m, b, and ℓ. The experimental values are now given.

a. Static Lift

The dimensionless quantity c is a measure of the lateral force proportional to angle of attack. This force is zero for perfect fluids; however, it has ponderable magnitude for real fluids. Experimental values are given in Fig. 17 for Reynolds number based on the length of the body. Included on the figure is the experimental value for a wind tunnel test of the airship "Shenandoah"(2). The basis of dimensionality is the equation:

$$\ell = c_\ell \frac{\rho}{2} U_o^2 A \quad . \tag{37}$$

The quantity A is the area of the circular cross section of the ellipsoidal body.

b. Damping Force due to Angular Velocity

The dimensionless quantity $(k_2 - k_1)$ is a measure of the lateral force due to angular velocity. Experimental and perfect fluid values are given in Fig. 18. The basis of dimensionality is the equation:

$$b = (k_2 - k_1) M_o U_o \quad . \tag{38}$$

c. Lateral Force due to Angular Acceleration

A dimensionless quantity c_a is defined as a measure of the lateral force due to angular acceleration. This quantity is zero for perfect fluids. The experimentally measured values are given in Fig. 19. The basis of dimensionality is the equation:

$$m = c_a \frac{\rho}{2} A (2a)^2 \quad . \tag{39}$$

Conclusions

The comparisons of the measured hydrodynamic reactions with the perfect fluid reactions are now given.

The static lift force is the principal real fluid force attributable entirely to the viscosity of the fluid. Its coefficient is plotted versus Reynolds number in Fig. 17. The magnitude agrees with other experimental data.[2] These coefficients were based on the intercept at zero frequency of oscillation in the data reduction curves of Fig. 8, 9, and 10. The curvature of these lines at the low frequencies of oscillation suggests a dynamic effect may be present; that is, the lift force proportional to instantaneous angle of attack is not completely independent of the angular velocity or angular acceleration.

The lateral force due to angular velocity is a perfect fluid force that depends on the difference of the virtual inertia coefficients of the body shape. In Fig. 18 it is seen that all of the experimentally determined values are higher than the perfect fluid values. The experimental values may be reduced about three percent by the addition of a correction for the effect of the spindle shield. The magnitude of the correction was estimated by placing a second shield in the tunnel on the other side of the model. It was assumed that the

effects of the two shields are additive, and the correction was estimated on this basis. This correction was not applied to the curves because it did not exceed the scatter of the experimental points; however, it is in the direction that decreases the difference between the measured real and perfect fluid forces. It is concluded that the real fluid force is less than five percent higher than the perfect fluid force on the basis of the measurements on the 7:1 and 3:1 aspect ratio bodies. The difference is about eight percent for the 5:1 aspect ratio.

The lateral force due to angular acceleration is a real fluid effect. From Fig. 19 it is seen that its dimensionless coefficient is roughly proportional to Reynolds number over the experimental range of tunnel velocities. Its magnitude is small at the low frequencies compared with the static lift force; at 10 cps it is comparable to the lift force.

The measurement of the angular quantities is made difficult by the large negative or destablizing static moment rate and low damping moment rate. The balance had to be operated at frequencies well below tha natural frequency of the system and the amplitude ratios of the drive and model motion changed from unity to about 1.4 over the frequency range of two to ten cps. The separation of the components of moment thus required the

differences of nearly equal quantities in many instances. The experimental static moment rate as shown in Fig. 14 agrees well with the perfect fluid values particularly at the higher fluid velocities where this reaction is large.

The experimental value of the coefficient of virtual moment of inertia exhibits a definite decrease with increasing tunnel velocity. The measurements of the 3:1 aspect ratio body should be disregarded completely; the magnitude of the moment of inertia of the body itself is large compared with the additional moment of inertia of the fluid. The decreasing value with increasing tunnel velocity is to be expected; it represents loss in the kinetic energy of motion in a real fluid due to its viscosity.

The damping moment or moment due to angular velocity is small compared with the static moment and moment of inertia reaction over the range of the experimental tests. Its perfect fluid value is zero. The real fluid value was so small that only an estimate of its maximum value could be determined.

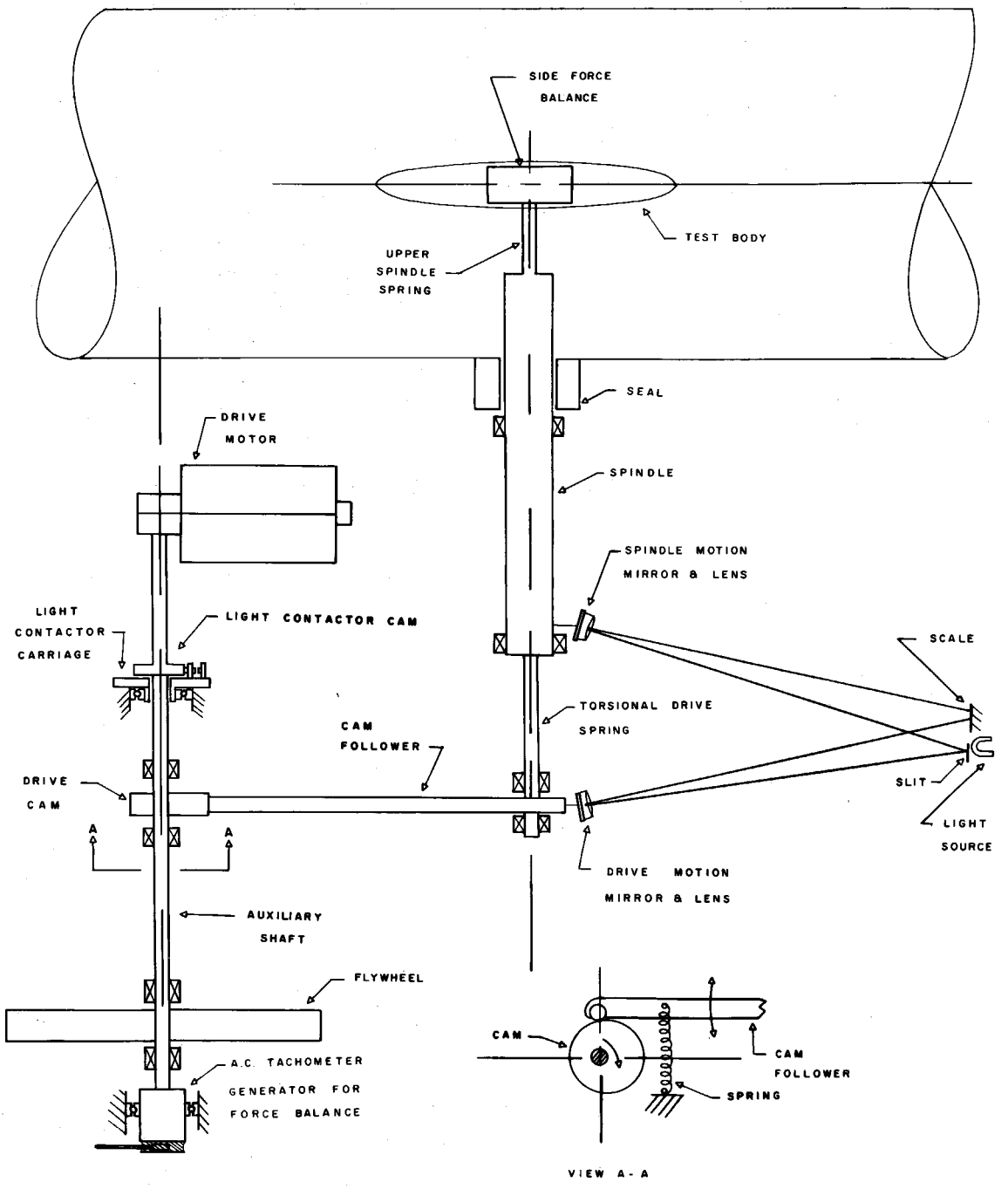

FIG. 1 - SCHEMATIC DIAGRAM OF ANGULAR BALANCE

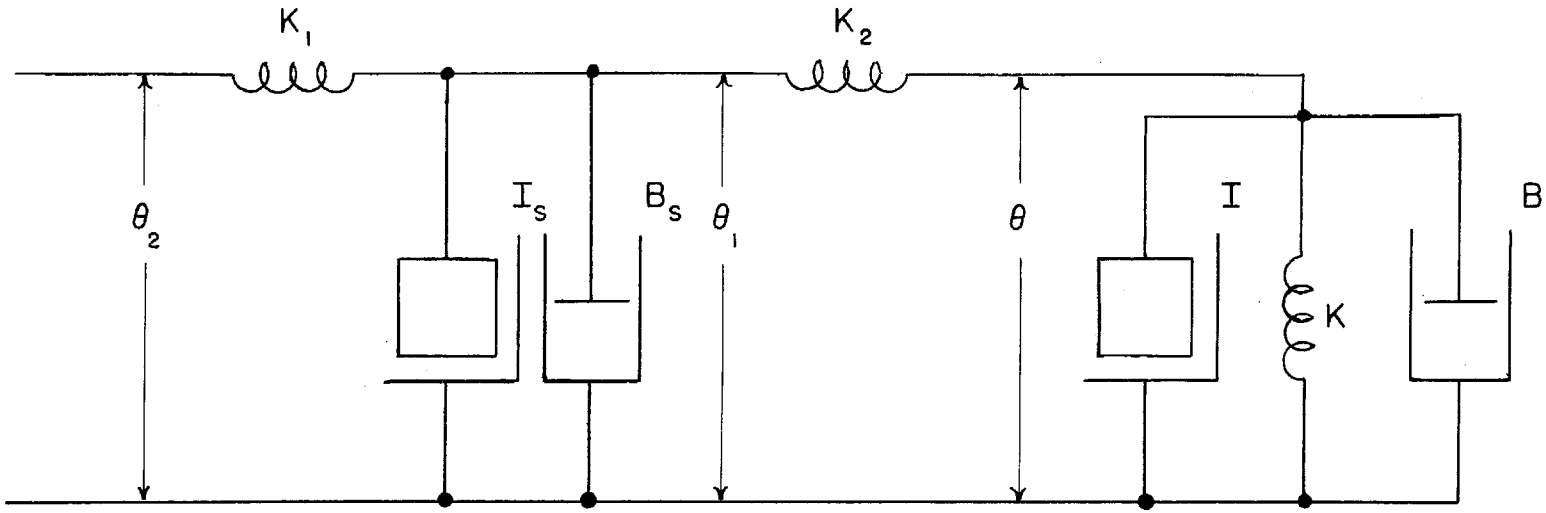

K_1	Drive spring rate	B_s	Damping rate of spindle seal
K_2	Spindle spring rate	I_s	Moment of inertia of spindle
K	Equivalent spring rate of fluid	θ	Motion of body
B	Equivalent damping rate of fluid	θ_1	Motion of spindle
I	Moment of inertia of body and fluid	θ_2	Motion of drive platform

Fig. 2 - Equivalent Mechanical Diagram of Angular Balance

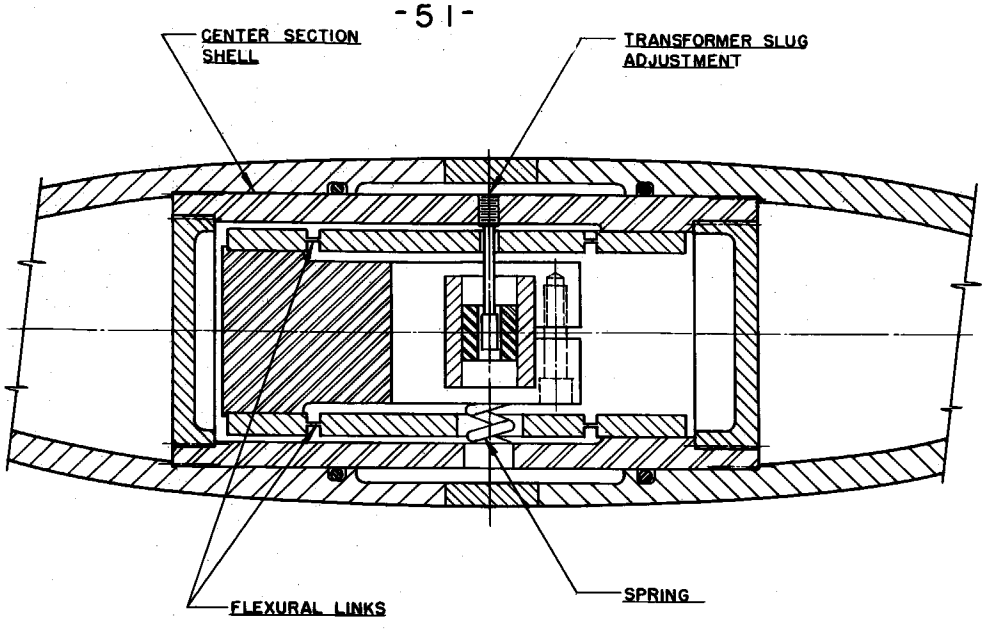

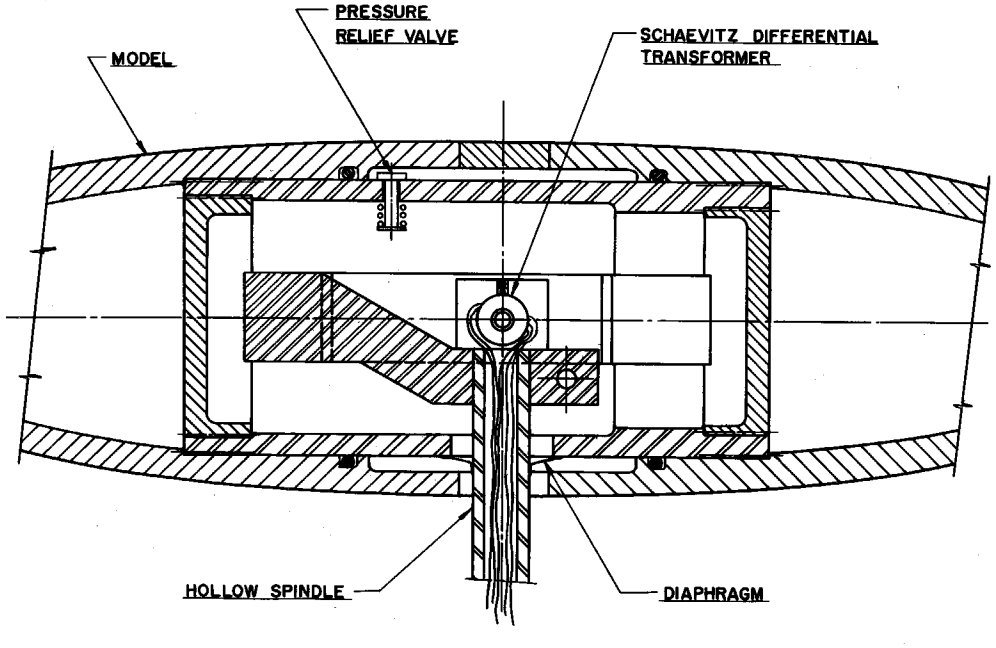

FIG. 3 - SCHEMATIC DIAGRAM OF SIDE FORCE BALANCE

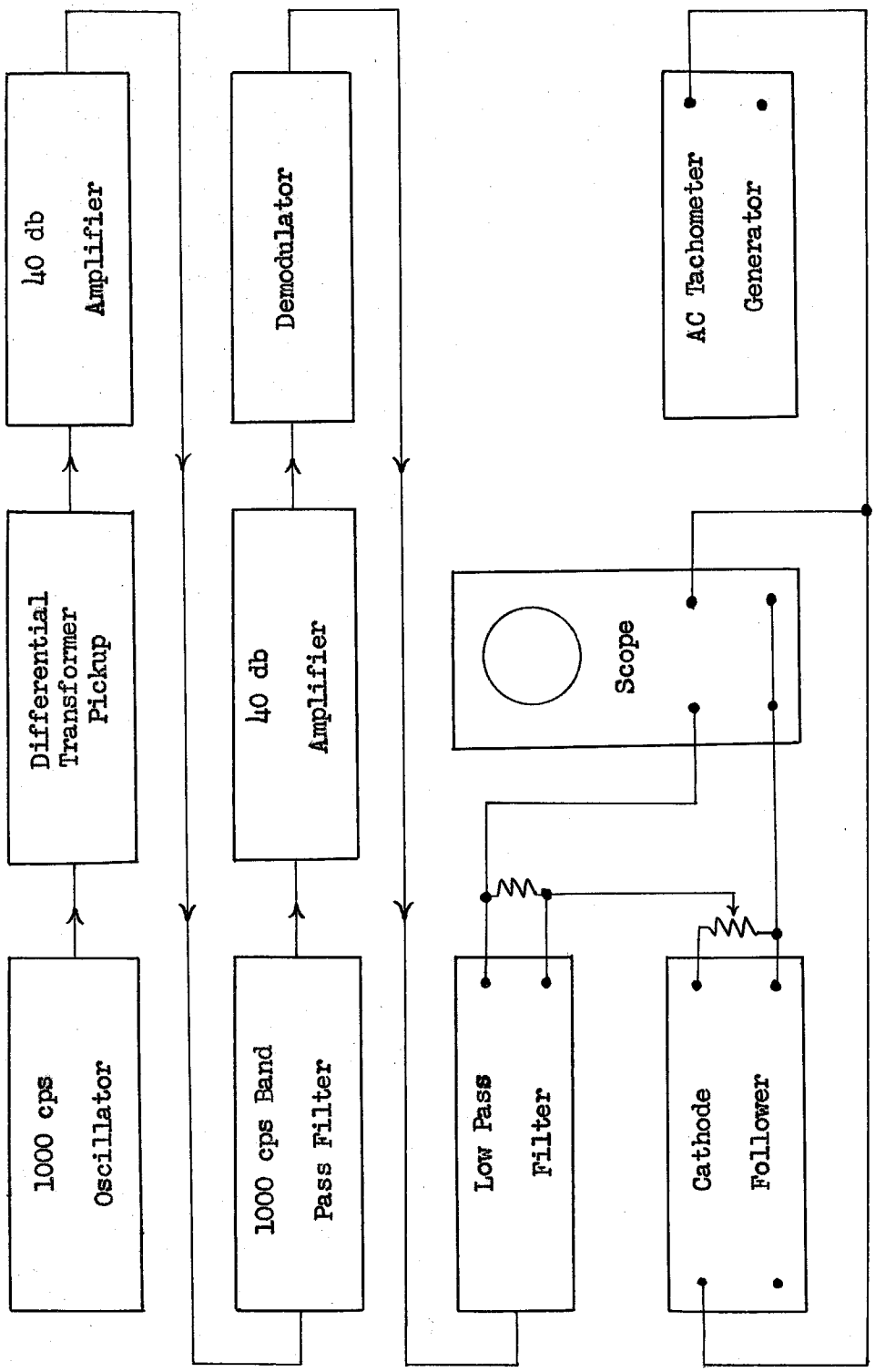

Fig. 4 - Block Diagram of Electronic Equipment for Side Force Balance

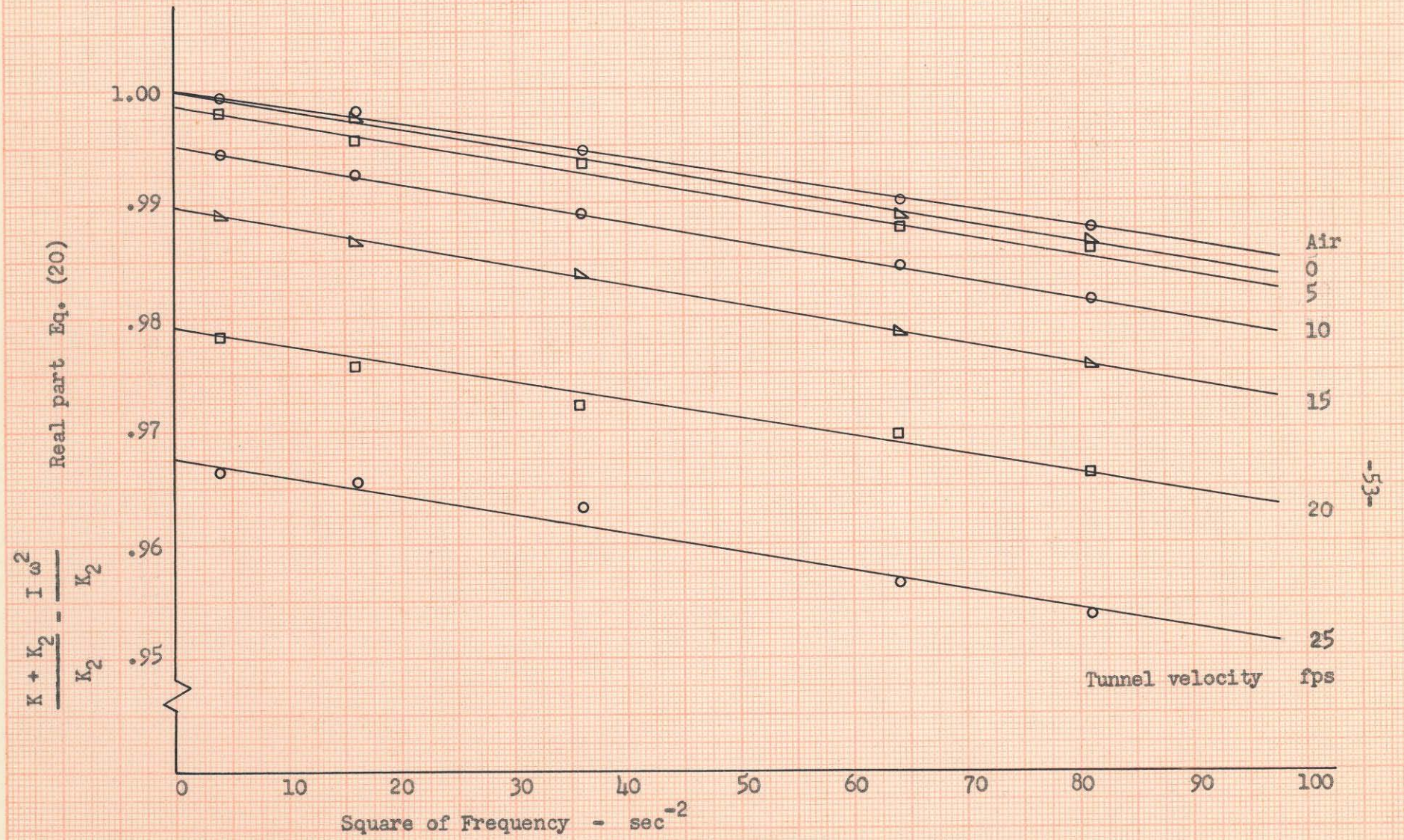

Fig. 5 - Data Reduction Curve - 3 : 1 Aspect Ratio

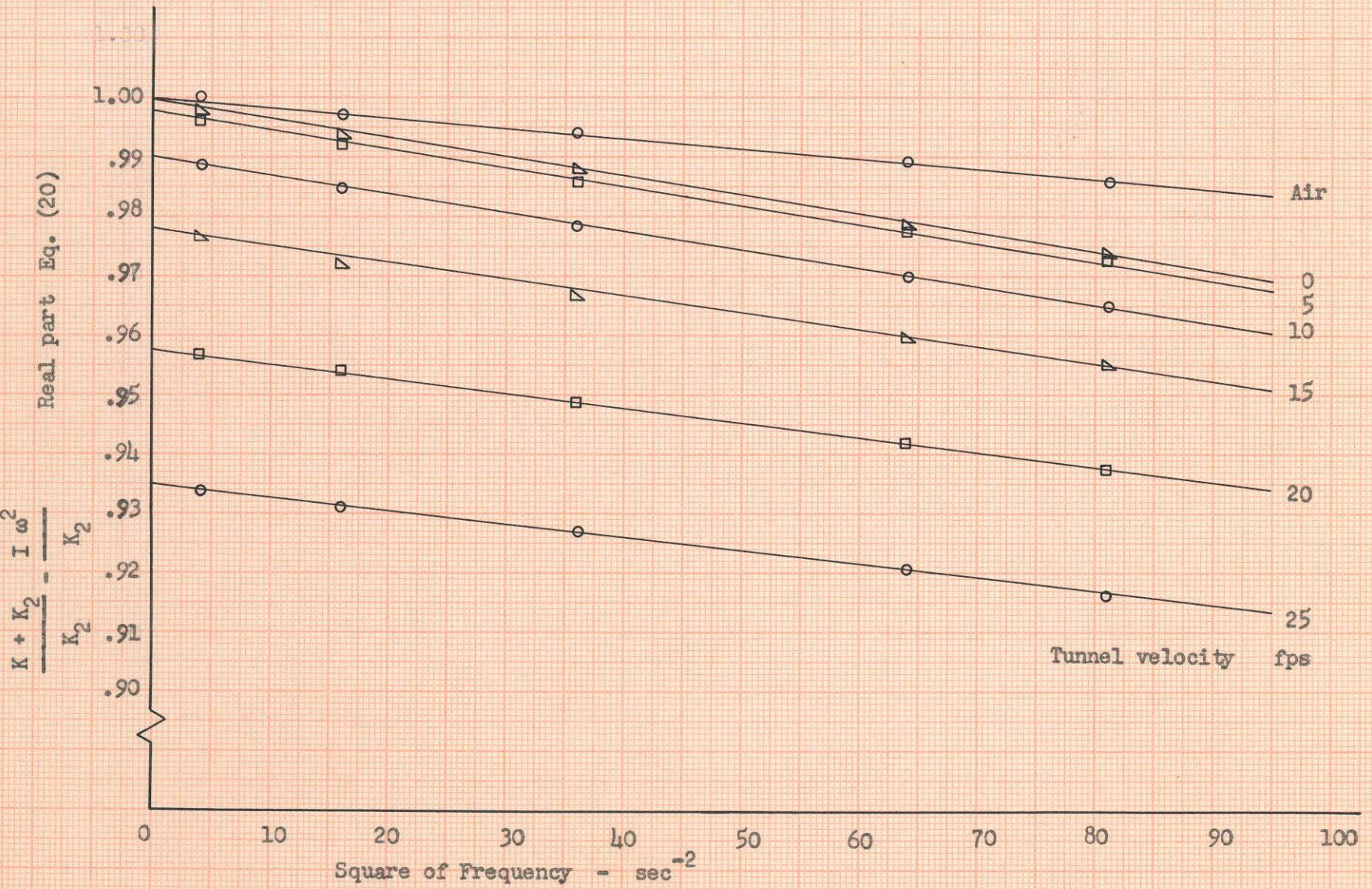

Fig. 6 - Data Reduction Curve - 5 : 1 Aspect Ratio

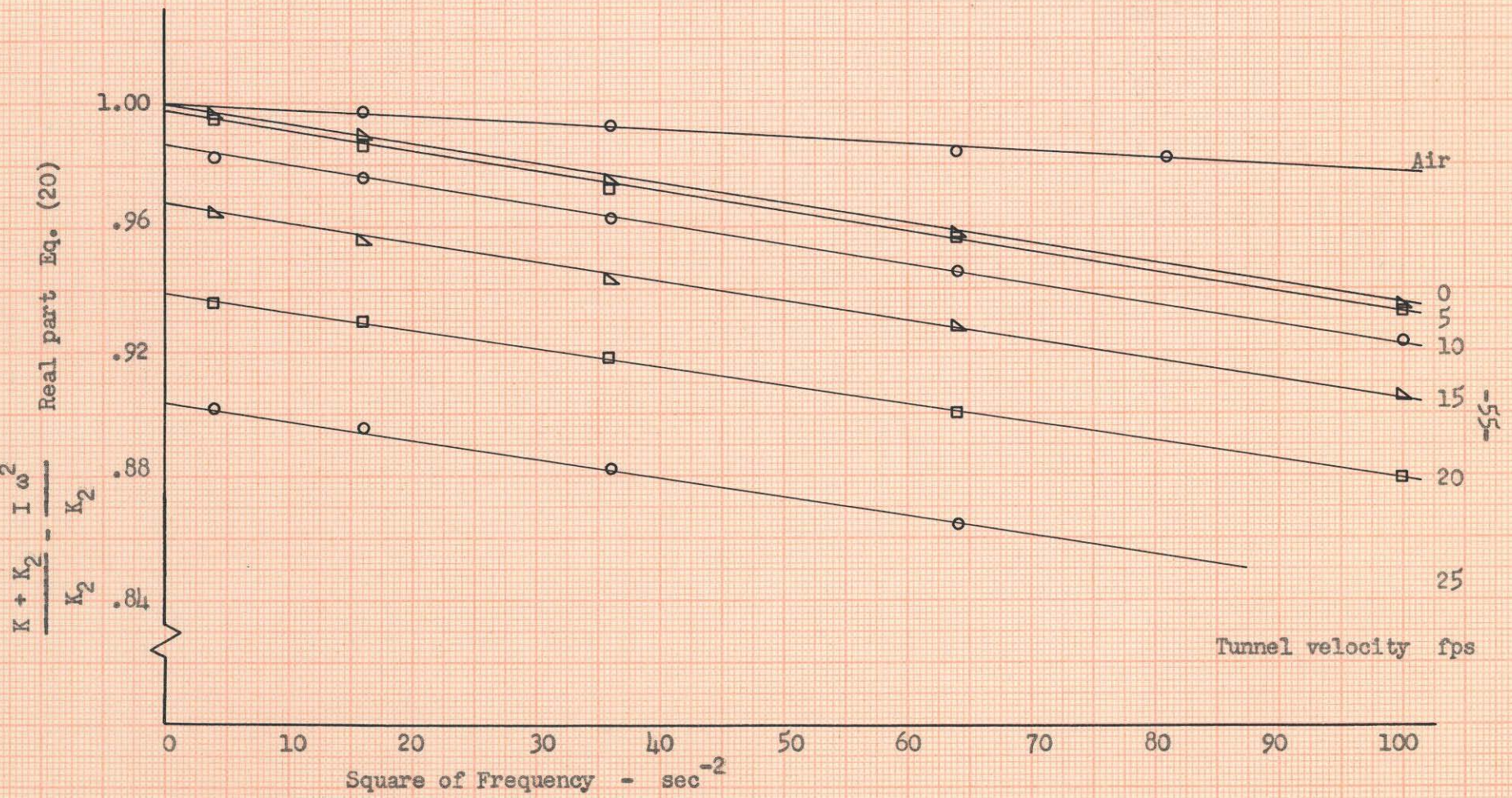

Fig. 7 - Data Reduction Curve - 7 : 1 Aspect Ratio

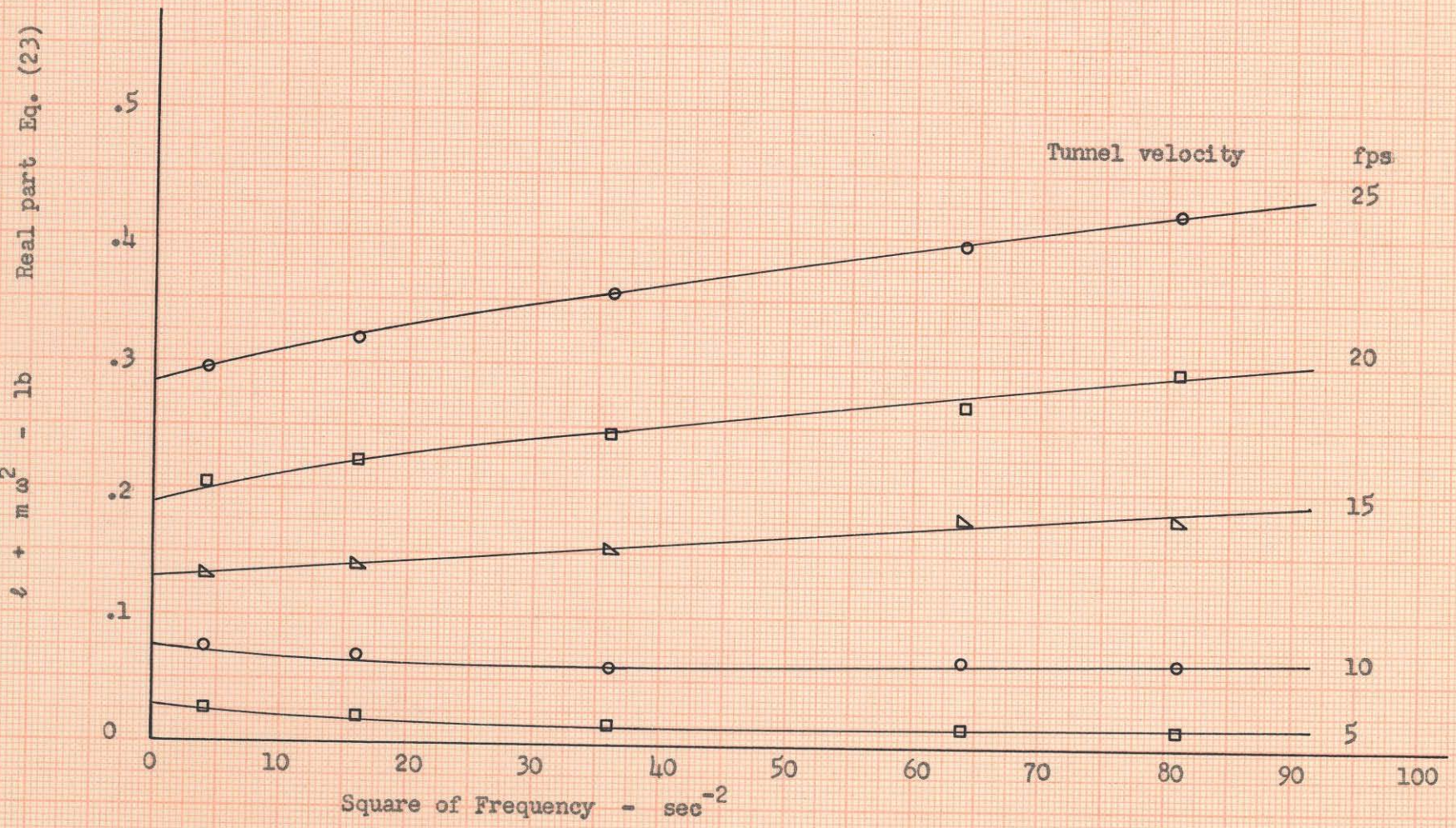

Fig. 8 - Data Reduction Curve - 3 : 1 Aspect Ratio

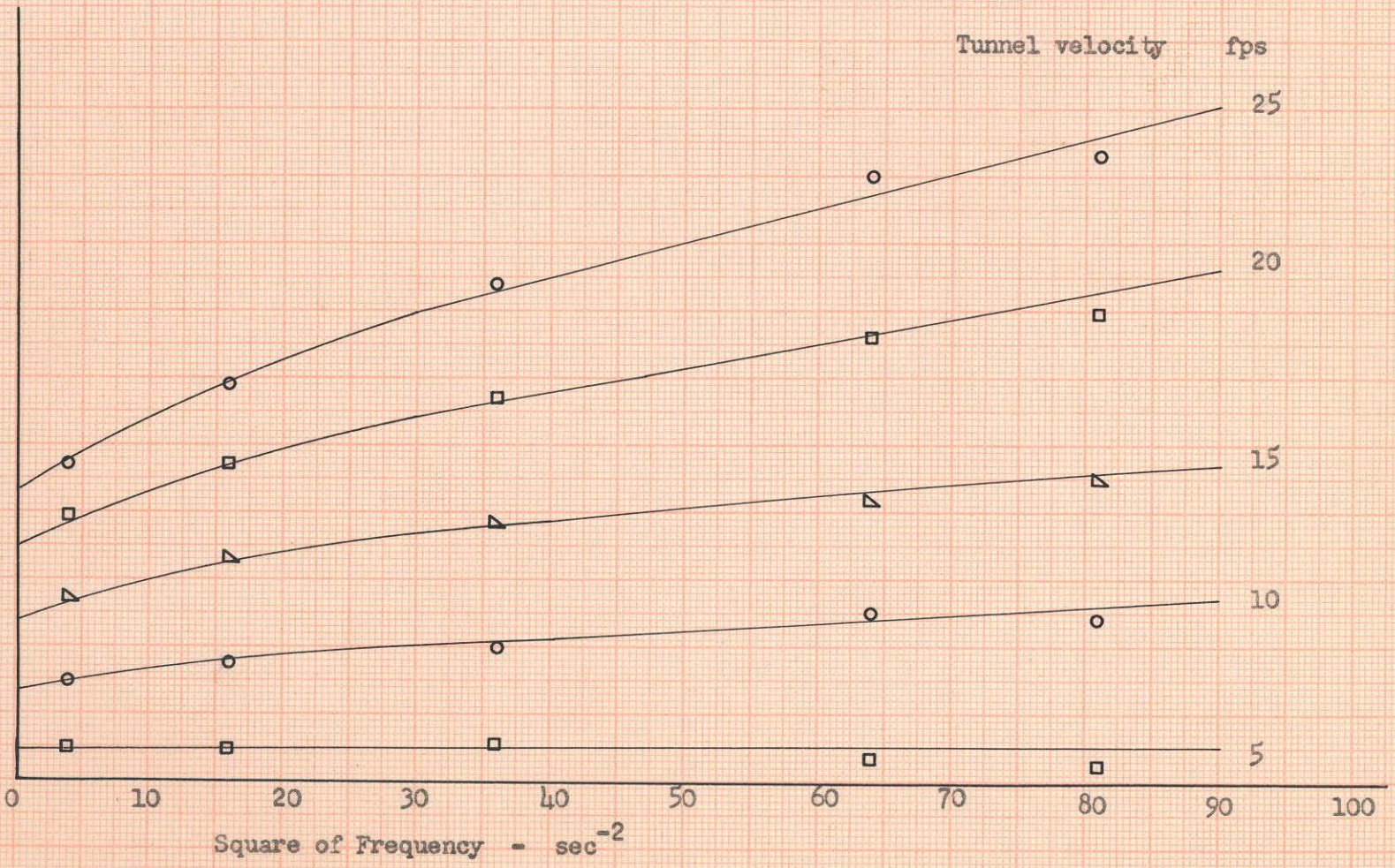

Fig. 9 - Data Reduction Curve - 5 : 1 Aspect Ratio

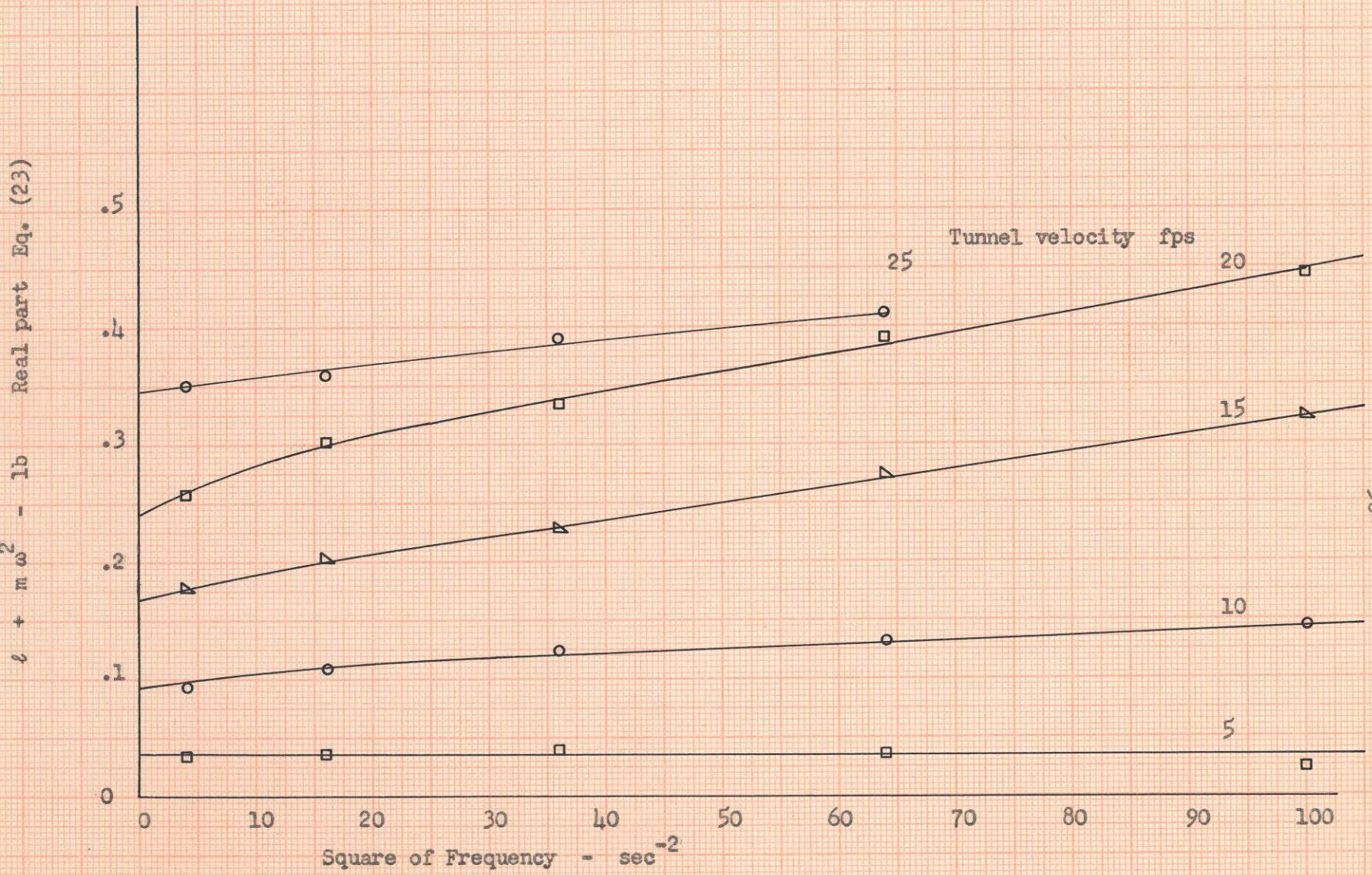

Fig. 10 - Data Reduction Curve - 7 : 1 Aspect Ratio

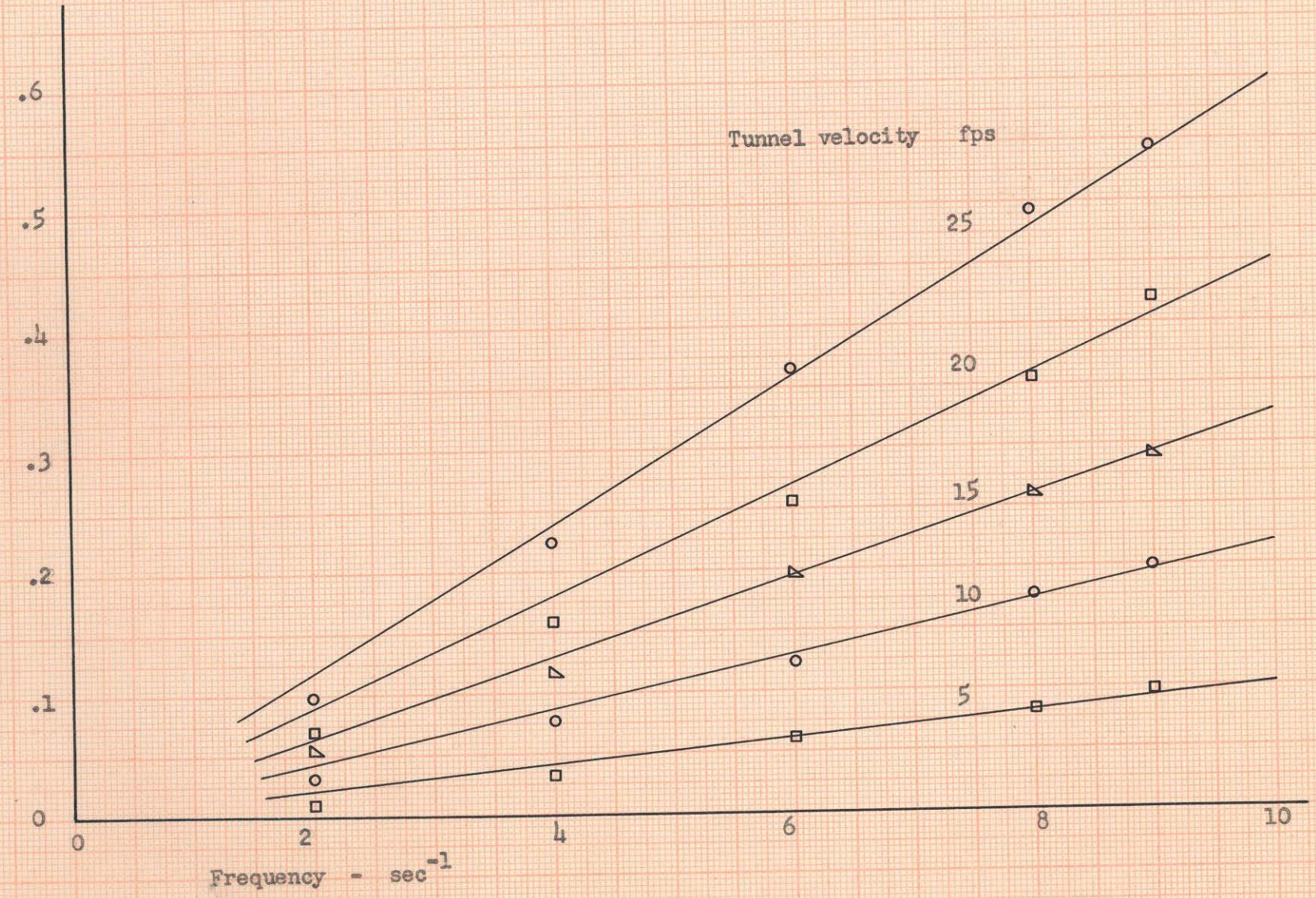

Fig. 11 - Data Reduction Curve - 3 : 1 Aspect Ratio

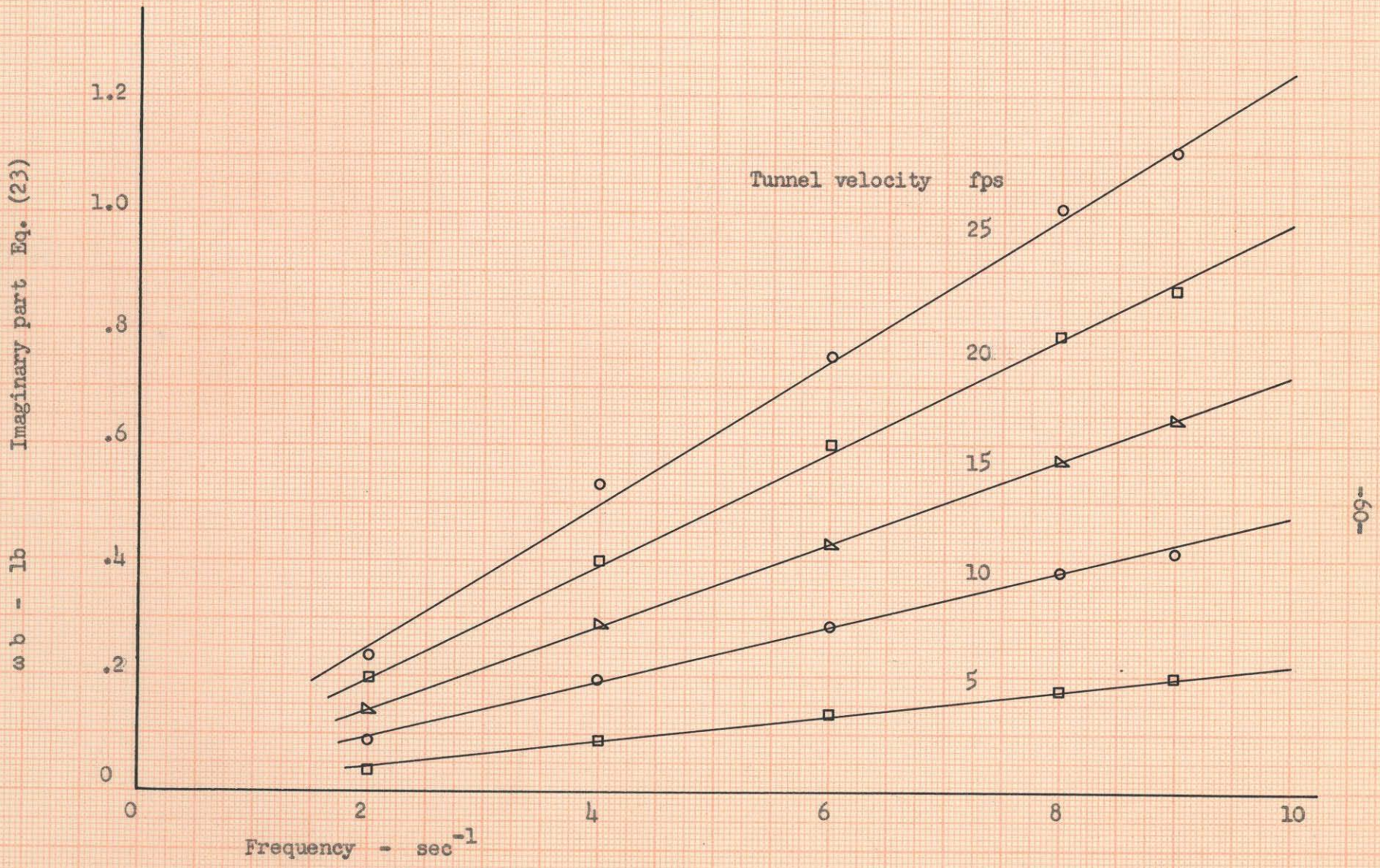

Fig. 12 - Data Reduction Curve - 5 : 1 Aspect Ratio

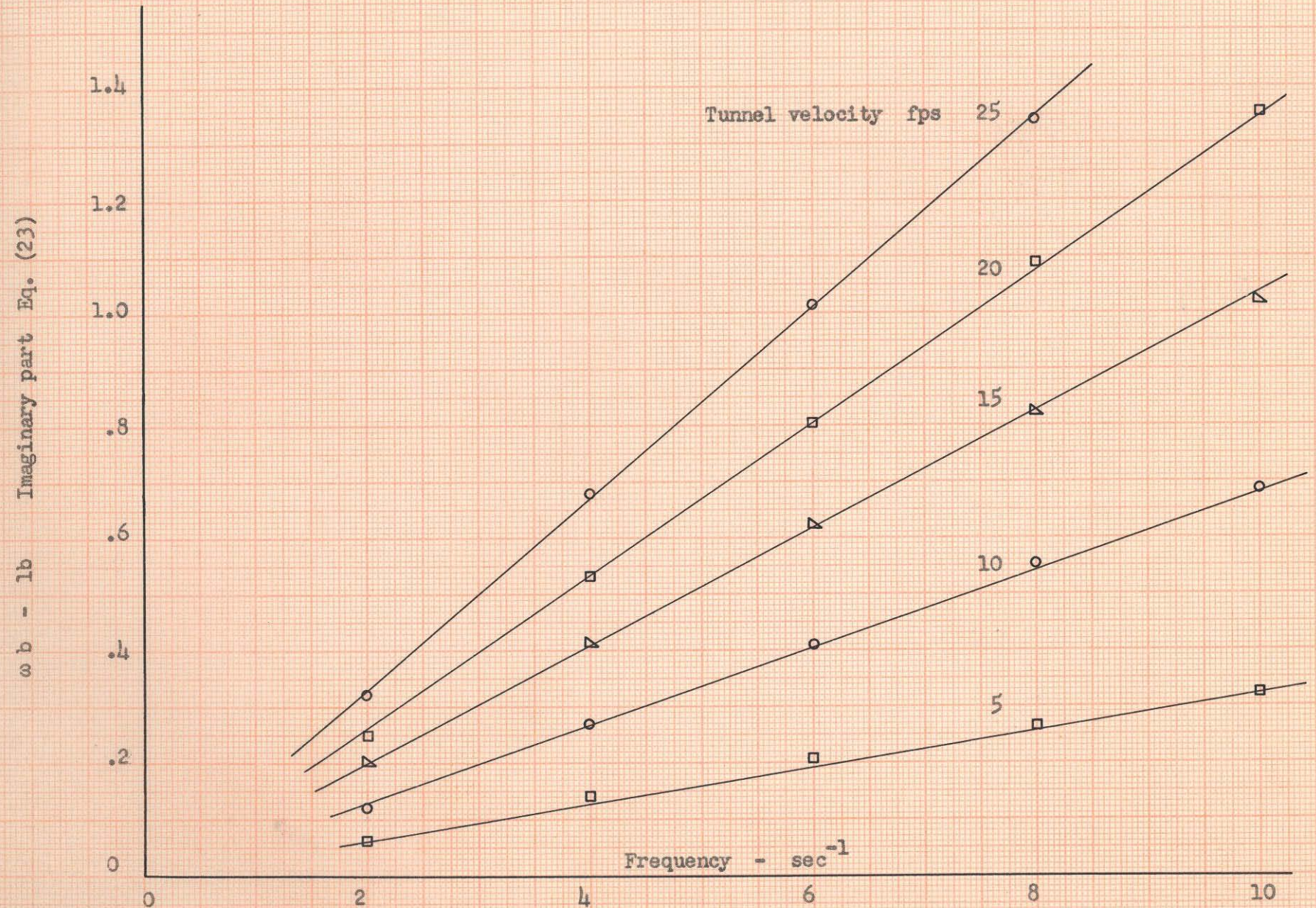

Fig. 13 - Data Reduction Curve - 7 : 1 Aspect Ratio

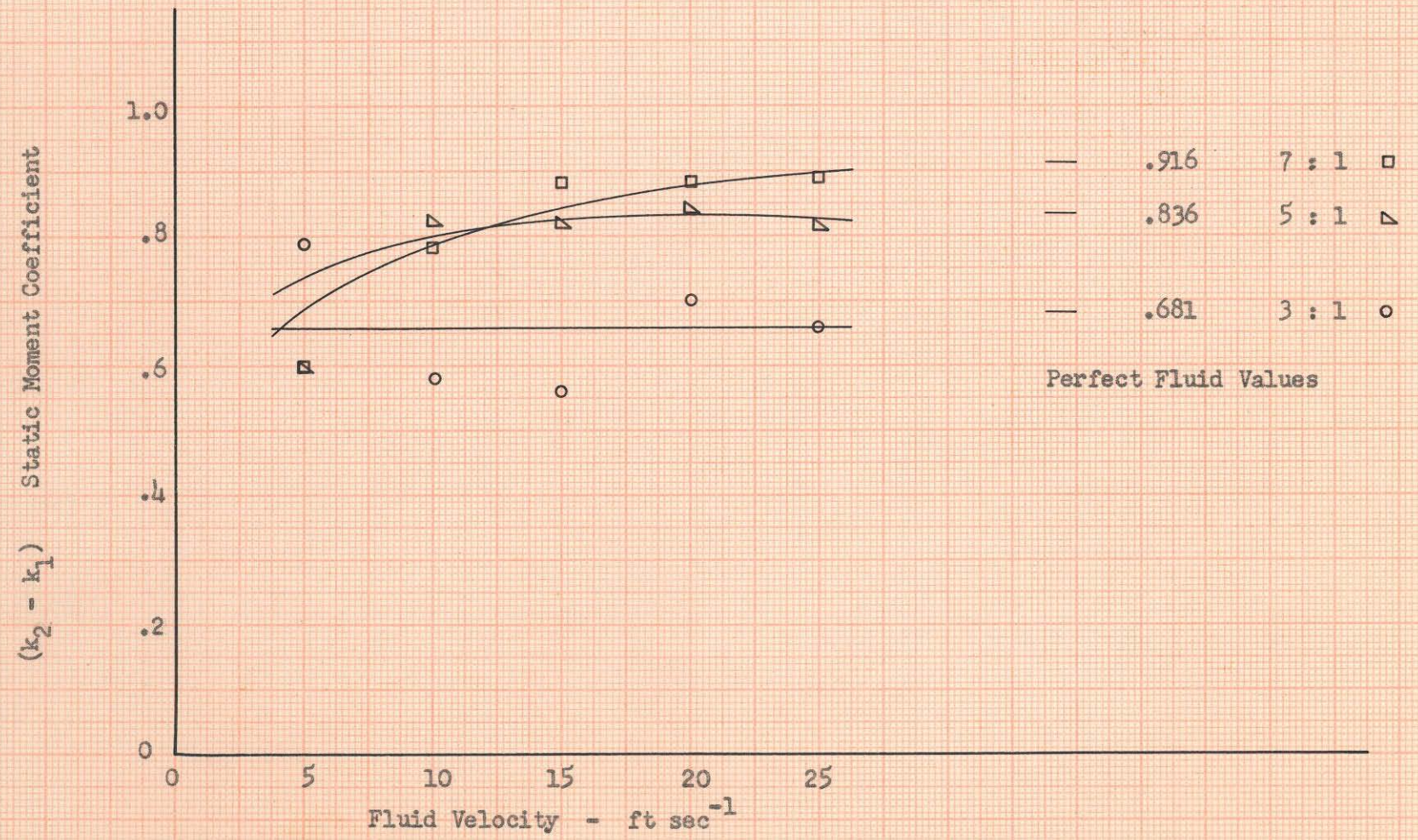

Fig. 14 - Static Moment Coefficient

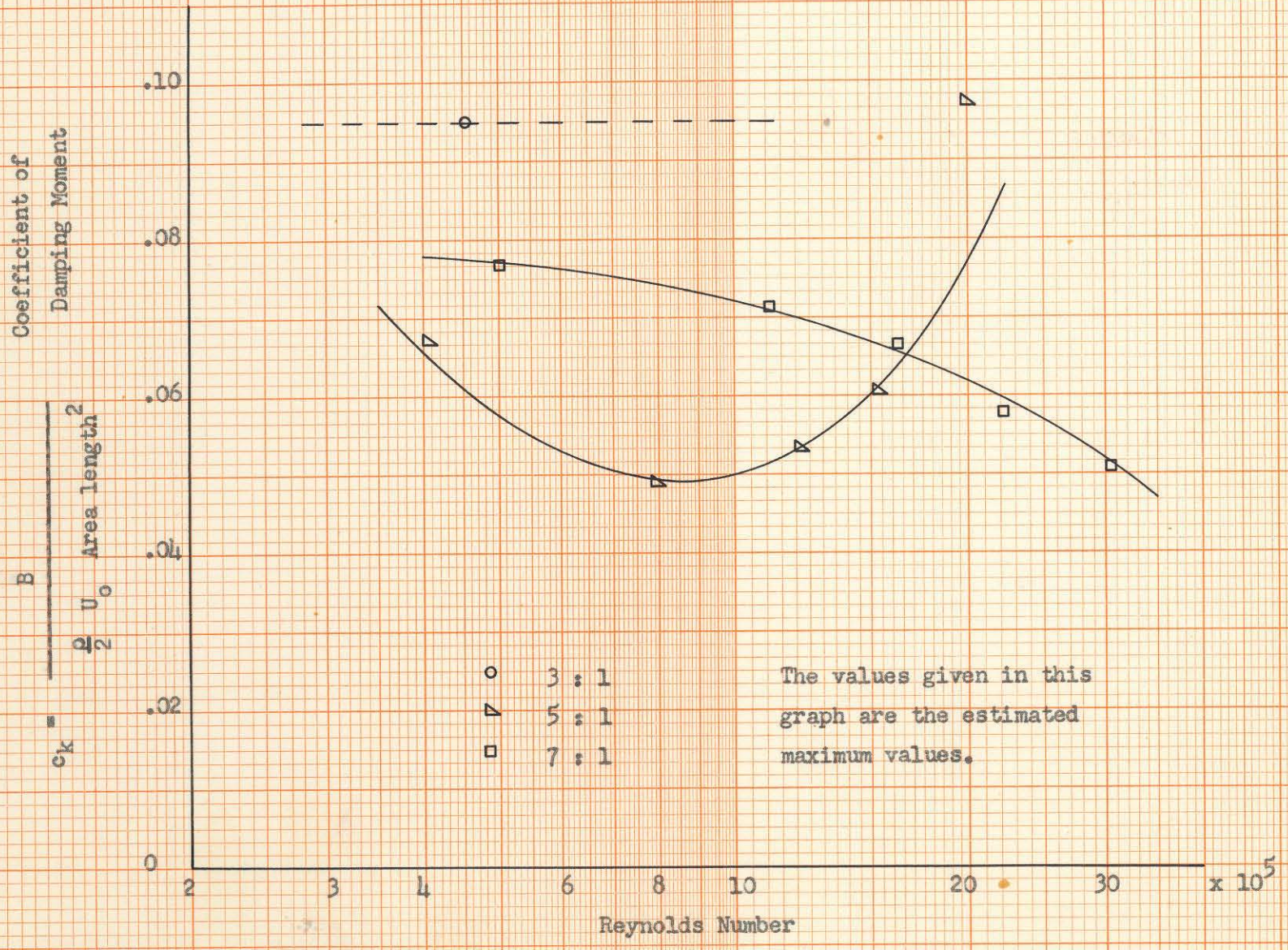

Fig. 15 - Moment Due to Angular Velocity

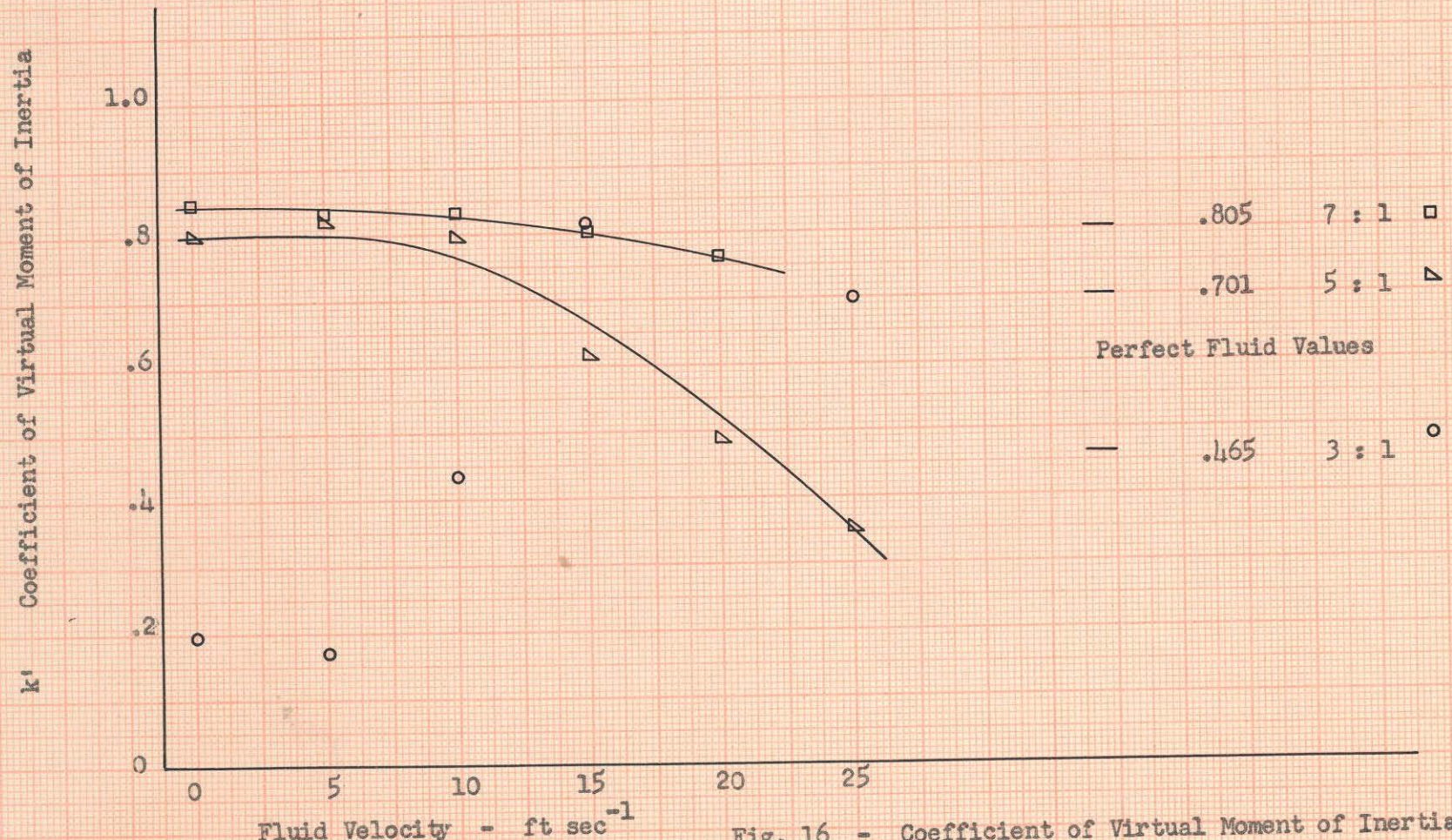

Fig. 16 - Coefficient of Virtual Moment of Inertia

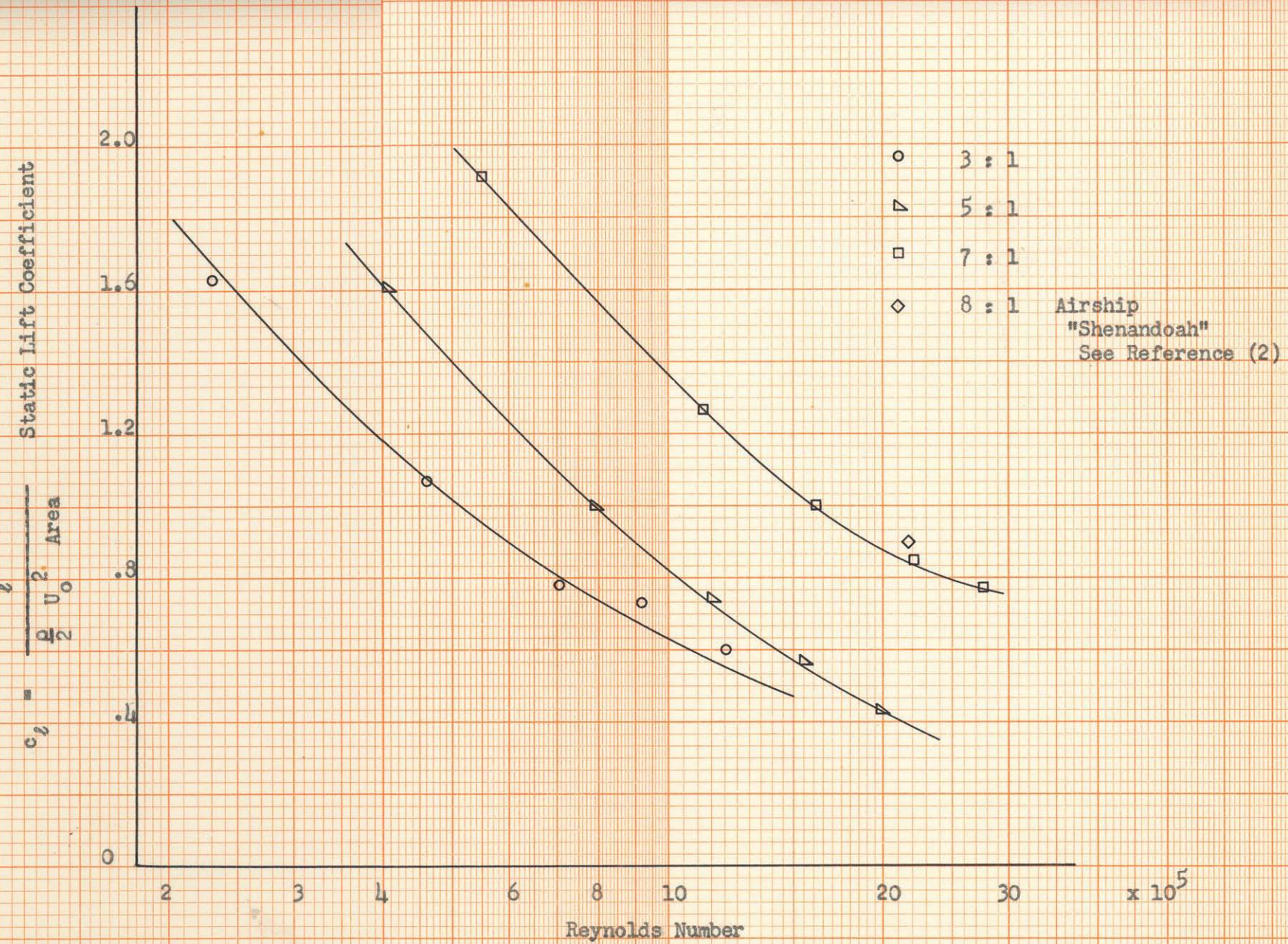

Fig. 17 - Static Lift Coefficient

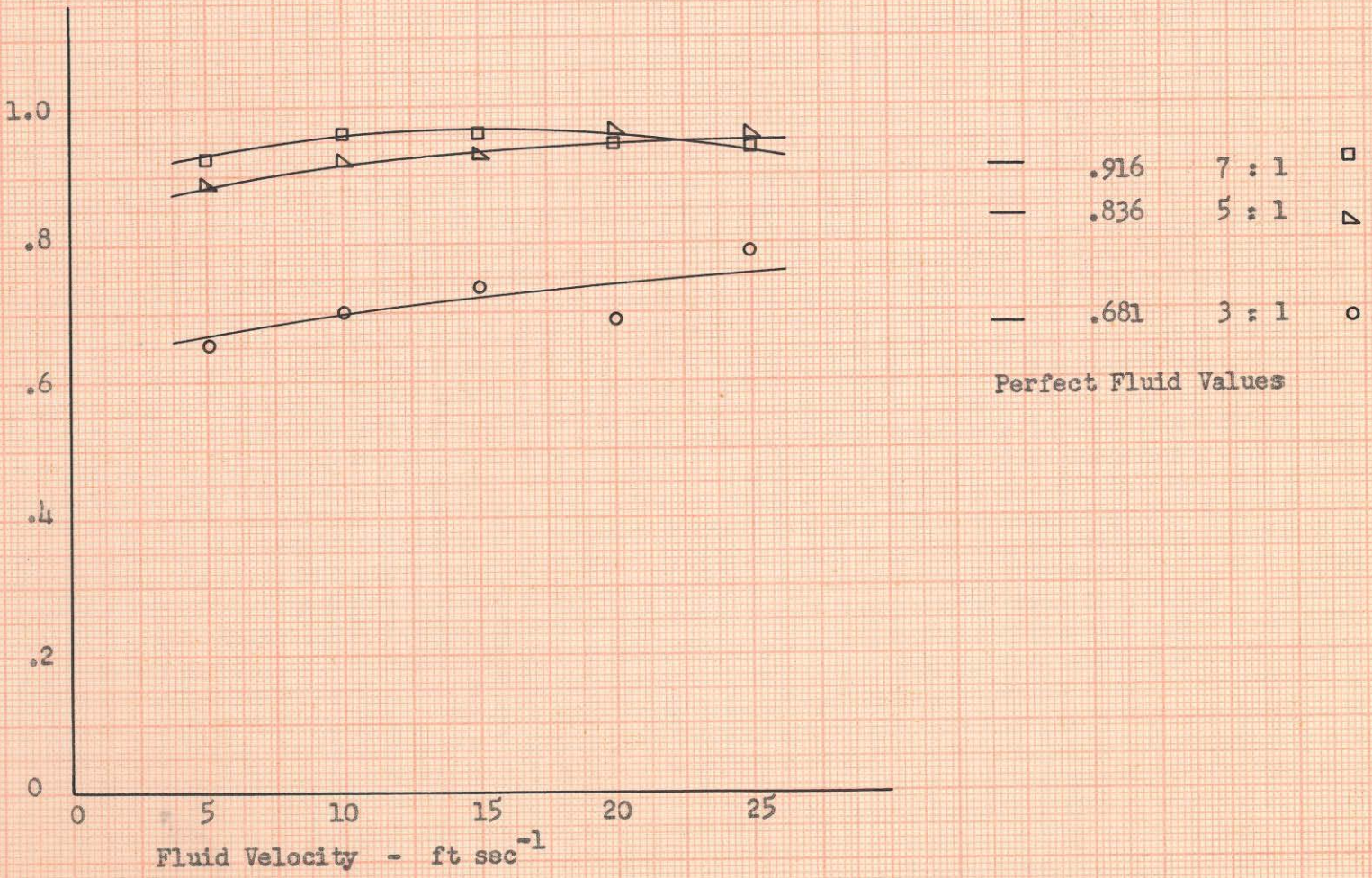

Fig. 18 - Lateral Force Due to Angular Velocity

Fig. 19 - Lateral Force Due to Angular Acceleration

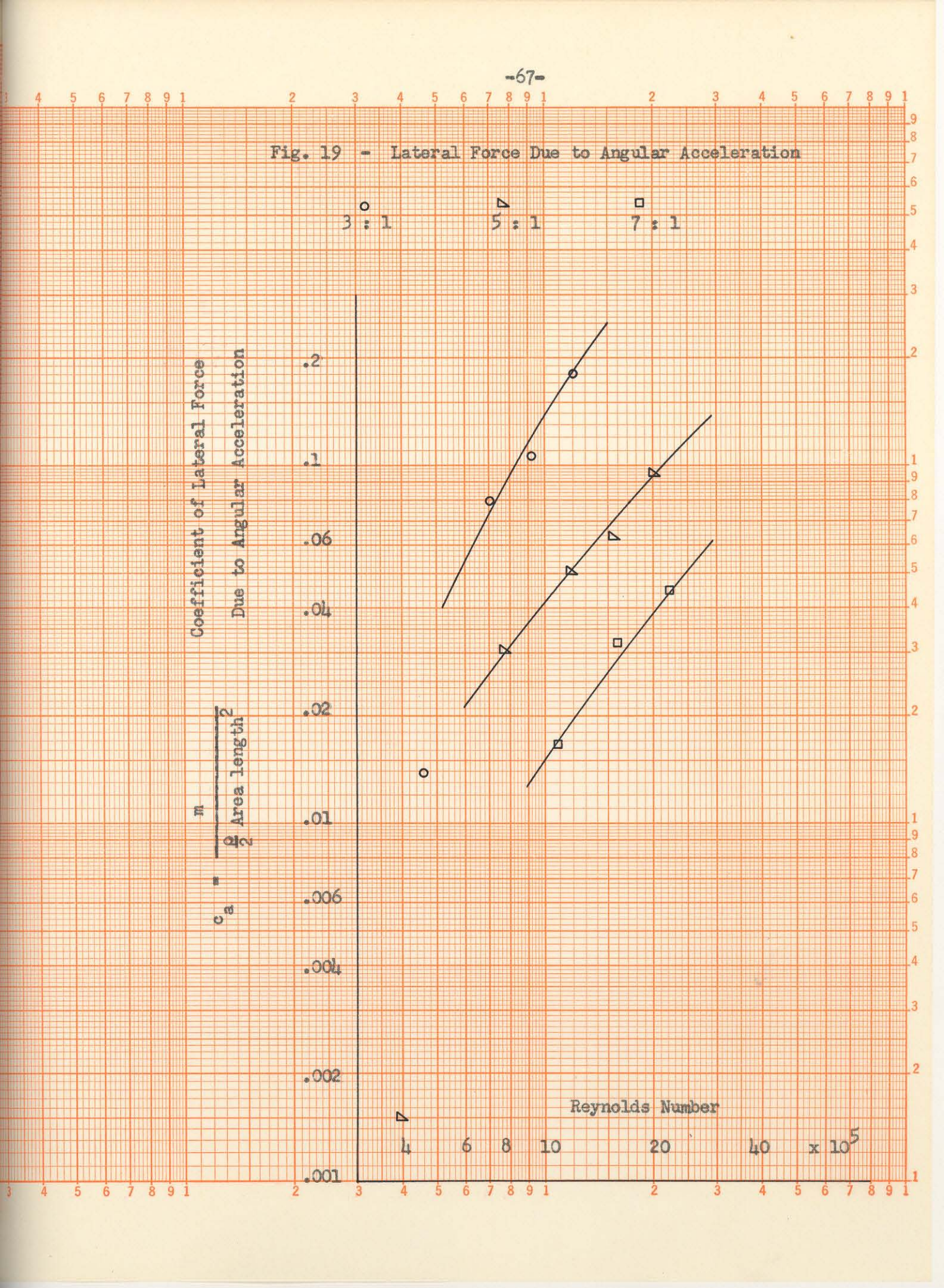

APPENDIX I

Notation

All quantities are in foot-pound-second units. (pound force)

x_o , y_o	inertial coordinates
x , y	body axes, fixed in body, origin at center of gravity or at geometric center for ellipsoids
θ	angle of x axis from x_o axis
u_o , v_o	velocity of body in inertial frame
u , v	velocity of body in inertial frame resolved along body axes
M	mass of body
I_b	moment of inertia of body
T_s	kinetic energy of motion of body
f_x , f_y	hydrodynamic forces exerted on body in inertial frame resolved along body axes
F_x , F_y	total external forces on body in space or on body and fluid system resolved along body axes
n	hydrodynamic moment exerted on body
N	total external moment on body in space or on body and fluid system

The other quantities are defined in the text as they appear; several of these are collected here.

a , b	semi-axes of prolate ellipsoid, a greater than b
M_o	mass of displaced fluid
I_o	moment of inertia of displaced fluid about origin of body axes

k_1, k_2, k'	virtual inertia coefficients of a prolate ellipsoid from Appendix III
p	pressure in fluid
ρ	density of fluid
$\bar{q}$	velocity of point in fluid
$\bar{q}_b$	velocity of point on surface of body
$\bar{q}_r$	relative velocity of fluid and body at a point on surface of body
m, b, ℓ	coefficients of real fluid reaction on body
I_f, B, K	defined in Eq. (14)
f	frequency of angular oscillation of model
A_o, A_1, A_2	amplitude of oscillation of model, spindle, drive platform
α_o, α_1, α_2	phase angle of model, spindle, drive motion
F_i	rms value of the lateral force on body
α_i	phase angle of lateral force on body
K_1 , K_2	torsion spring rate of drive spring and upper spindle spring
I_s	moment of inertia of spindle
B_s	angular damping rate of spindle seal

Equations of Motion of a Rigid Body in Space

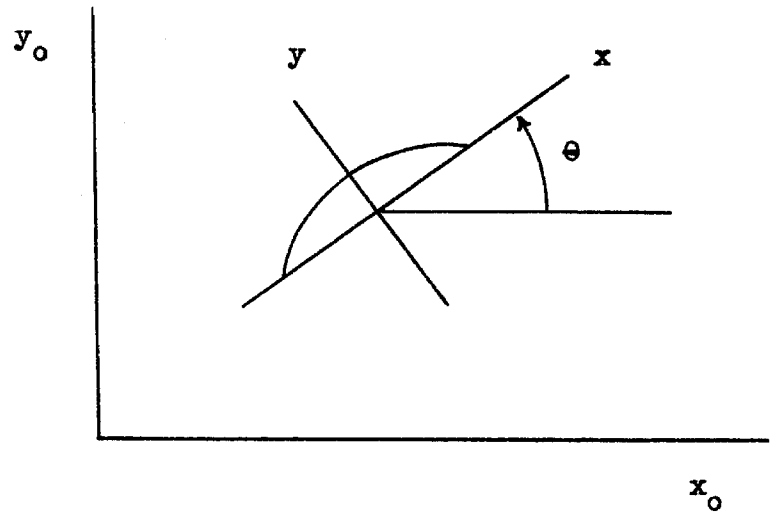

Kinematics of two dimensional motion:

$$u = u_o \cos\theta + v_o \sin\theta$$

$$v = -u_o \sin\theta + v_o \cos\theta$$

$$F_x = F_{x_o} \cos\theta + F_{y_o} \sin\theta$$

$$F_y = -F_{x_o} \sin\theta + F_{y_o} \cos\theta \quad .$$

The equations of motion may be written from Lagrange's equation or for this simple case from Newton's law.

$$F_{x_o} = M\dot{u}_o \quad , \quad F_{y_o} = M\dot{v}_o \quad , \quad N = I_b\ddot{\theta}$$

$$F_x = M(\dot{u} - v\dot{\theta}) \quad , \quad F_y = M(\dot{v} + u\dot{\theta})$$

These last two equations can be derived from the first two by using the kinematic relationships. They may also be arrived at directly by using Kirchhoff's form of Lagrange's equation which is applicable to this case of moving axes.

Kirchhoff's equations for two dimensional motion are

$$F_x = \frac{d}{dt}\frac{\partial T}{\partial u} - \dot{\theta}\frac{\partial T}{\partial v} \quad ,$$

$$F_y = \frac{d}{dt}\frac{\partial T}{\partial v} + \dot{\theta}\frac{\partial T}{\partial u} \quad ,$$

$$N = \frac{d}{dt}\frac{\partial T}{\partial \dot{\theta}} - v\frac{\partial T}{\partial u} + u\frac{\partial T}{\partial v} \quad .$$

The kinetic energy, T , is a function of u, v, and $\dot{\theta}$ for this case. These equations may be derived by application of the kinematic conditions to Lagrange's equation. The forces and moment are still measured in the x_o , y_o inertial system; they are resolved along the instantaneous directions defined by the angle θ.

APPENDIX II

Equations of Motion of a Rigid Body in an Infinite Volume of Frictionless Fluid at Rest at Infinity

In chapter XVII of the text of Milne-Thomson [1], the equations of motion are derived from the rate of change of the impulse of the system. The following presentation is taken from section 17.60 in which the same equations are arrived at in a heuristic manner.

Consider the motion of a system of rigid bodies moving in a frictionless fluid that is contained in a fixed envelope E. Describe the configuration of the bodies by the generalized coordinates $(q_1, q_2, \ldots q_n)$. The solids form a holonomic system. Let the position vector to a point of a solid body be $\bar{r}$.

$$\bar{r} = \bar{r}\ (q_1, \ldots q_n) \tag{1}$$

$$\bar{v} = \dot{\bar{r}} = \sum i \frac{\partial \bar{r}}{\partial q_i} \dot{q}_i = \sum i\ \bar{\alpha}_i\ \dot{q}_i \tag{2}$$

$$\frac{\partial \bar{v}}{\partial \dot{q}_i} = \frac{\partial \bar{r}}{\partial q_i} \tag{3}$$

Consider a virtual motion described by the velocity $\frac{Dq_i}{Dt}$. Let $\frac{DW}{Dt}$ be the rate of doing work. Let $\bar{F} = m\,\bar{r}$ be the total force on P.

$$\frac{D\bar{r}}{Dt} = \sum i \frac{\partial \bar{r}}{\partial q_i} \frac{Dq_i}{Dt} \tag{4}$$

$$\frac{DW}{Dt} = \sum_P \bar{F} \frac{D\bar{r}}{Dt} = \sum_{P,i} \bar{F} \frac{\partial \bar{r}}{\partial q_i} \frac{Dq_i}{Dt} = \sum i\ Q_{s,i} \frac{Dq_i}{Dt} \tag{5}$$

The $Q_{s,i}$ are the components of the generalized force.

$$Q_{s,i} = \Sigma_P \bar{F} \frac{\partial \bar{r}}{\partial q_i} = \Sigma_P m \ddot{\bar{r}} \frac{\partial \bar{r}}{\partial q_i}$$

$$= \frac{d}{dt} \Sigma_P m \dot{\bar{r}} \frac{\partial \bar{r}}{\partial q_i} - \Sigma_P m \dot{\bar{r}} \frac{d}{dt} \frac{\partial \dot{\bar{r}}}{\partial q_i} \qquad (6)$$

The kinetic energy of the solids is given by:

$$T_s = \frac{1}{2} \Sigma_P m \dot{\bar{r}} \dot{\bar{r}} \quad . \qquad (7)$$

Equation (6) now becomes:

$$Q_{s,i} = \frac{d}{dt} \frac{\partial T_s}{\partial \dot{q}_i} - \frac{\partial T_s}{\partial q_i} \quad . \qquad (8)$$

This is Lagrange's equation for the solids.

The fluid is not a holonomic system; that is each particle of fluid is not defined by an explicit equation. The fluid motion is assumed to be due entirely to the motion of the solids and would cease if the solids were brought to rest. The fluid motion thus satisfies the conditions:

$$\nabla^2 \phi = 0, \qquad \bar{v} = -\bar{\nabla} \phi \qquad (9)$$

$$\frac{\partial \phi}{\partial n} = 0 \quad \text{at the envelope E,} \qquad (10)$$

$$-\frac{\partial \phi}{\partial n} = V_n = \text{normal component of velocity at the boundaries of the solids.} \qquad (11)$$

But V_n is a linear function of q_i. Therefore,

$$\phi = \Sigma_i \phi_i \dot{q}_i \quad , \qquad (12)$$

where ϕ_i is a function of the generalized coordinates but not of

the generalized velocities; and

$$-\bar{\nabla}\phi = \bar{v} = -\sum_i \frac{\partial \phi_i}{\partial \bar{r}} \dot{q}_i \quad , \tag{13}$$

$$\frac{\partial \bar{v}}{\partial \dot{q}_i} = -\frac{\partial \phi_i}{\partial \bar{r}} \quad . \tag{14}$$

The kinetic energy of the fluid is given by:

$$T_L = \frac{1}{2} \int \rho \, \bar{v} \, \bar{v} \, d\tau \tag{15}$$

$$\frac{\partial T_L}{\partial \dot{q}_i} = \int \rho \, \bar{v} \frac{\partial \bar{v}}{\partial \dot{q}_i} \, d\tau = -\int \rho \, \bar{v} \frac{\partial \phi_i}{\partial \bar{r}} \, d\tau \tag{16}$$

The equation of motion for a fluid particle is

$$\bar{F} = \rho \dot{\bar{v}} \quad . \tag{17}$$

For the same virtual motion defined for the solids, the virtual velocity of the fluid is given by:

$$\bar{V} = -\bar{\nabla}\phi = -\sum_i \frac{\partial \phi_i}{\partial \bar{r}} \frac{Dq_i}{Dt} \quad . \tag{18}$$

Since $\frac{D}{Dt}$ and $\frac{d}{dt}$ are independent operators, Eq. (13) and (18) give

$$\frac{d\bar{V}}{dt} = \frac{D\bar{v}}{Dt} \quad . \tag{19}$$

The generalized force and rate of doing work are given by:

$$\frac{DW}{Dt} = \int \bar{F} \, \bar{V} \, d\tau = \sum_i \int \bar{F} \frac{\partial \phi_i}{\partial \bar{r}} \frac{Dq_i}{Dt} \, d\tau = \sum_i Q_{L,i} \frac{Dq_i}{Dt} \, , \tag{20}$$

$$Q_{L,i} = -\int \bar{F} \frac{\partial \phi_i}{\partial \bar{r}} \, d\tau = -\int \rho \dot{\bar{v}} \frac{\partial \phi_i}{\partial \bar{r}} d\tau \, . \qquad (21)$$

Now:

$$\int \rho \bar{v} \bar{V} \, d\tau = \Sigma_i \int \rho v \frac{\partial \phi_i}{\partial \bar{r}} \frac{Dq_i}{Dt} d\tau = \Sigma_i \frac{\partial T_L}{\partial \dot{q}_i} \frac{Dq_i}{Dt} \, . \qquad (22)$$

Differentiate this with respect to time.

$$\int \rho \dot{\bar{v}} \bar{V} \, d\tau + \int \rho \bar{v} \dot{\bar{V}} \, d\tau = \Sigma_i \frac{d}{dt} \frac{\partial T_L}{\partial \dot{q}_i} \frac{Dq_i}{Dt} + \Sigma_i \frac{\partial T_L}{\partial q_i} \frac{D\dot{q}_i}{Dt} \, . \qquad (23)$$

But:

$$\int \rho \bar{v} \dot{\bar{V}} \, d\tau = \int \rho \bar{v} \frac{D\bar{v}}{Dt} d\tau = \frac{D}{Dt} \int \frac{1}{2} \rho \bar{v} \bar{v} \, d\tau = \frac{D}{Dt} T_L$$

$$= \Sigma_i \frac{\partial T_L}{\partial q_i} \frac{Dq_i}{Dt} + \Sigma_i \frac{\partial T_L}{\partial \dot{q}_i} \frac{D\dot{q}_i}{Dt} \, . \qquad (24)$$

When Eq. (18), (21), (23), and (24) are combined, the result is

$$Q_{L,i} \frac{Dq_i}{Dt} = -\int \rho \dot{\bar{v}} \frac{\partial \phi_i}{\partial \bar{r}} \frac{Dq_i}{Dt} d\tau = \int \rho \dot{\bar{v}} \bar{V} \, d\tau$$

$$= \Sigma_i \frac{d}{dt} \frac{\partial T_L}{\partial \dot{q}_i} \frac{Dq_i}{Dt} + \Sigma_i \frac{\partial T_L}{\partial \dot{q}_i} \frac{D\dot{q}_i}{Dt} - \int \rho \bar{v} \dot{\bar{V}} \, d\tau$$

$$= \Sigma_i \frac{d}{dt} \frac{\partial T_L}{\partial \dot{q}_i} \frac{Dq_i}{Dt} - \Sigma_i \frac{\partial T_L}{\partial q_i} \frac{Dq_i}{Dt} \, , \qquad (25)$$

and

$$\Sigma_i \left\{ Q_{L,i} - \frac{d}{dt} \frac{\partial T_L}{\partial \dot{q}_i} + \frac{\partial T_L}{\partial q_i} \right\} \frac{Dq_i}{Dt} = 0 \, . \qquad (26)$$

Since the $\frac{Dq_i}{Dt}$ are independent, Eq. (26) reduces to Lagrange's equation which is seen to hold for the liquid also.

Now the only forces on the system that can contribute to the virtual power in a virtual motion are external forces and forces on the envelope E. These latter can not contribute since the envelope does not move. Thus the total external force on the fluid and body system is given by Lagrange's equation when the total kinetic energy of the body and fluid sysyem is used.

The arbitrarily located envelope E may now be taken as large as desired. When it is allowed to go to infinity, no condition of the solution is violated. The kinetic energy in the fluid is finite and is given by a homogeneous quadratic form in the linear and angular velocities of the solids.

For the two dimensional motion of a single symmetrically shaped body such as a prolate ellipsoid moving with its long axis in the plane of motion, the kinetic energies are

$$2T_s = M u^2 + M v^2 + I_b \omega^2 \quad , \tag{27}$$

$$2T_L = A u^2 + B v^2 + R \omega^2 \quad . \tag{28}$$

Since the kinetic energies are independent of x_o and y_o, Kirchhoff's form of Lagrange's equation may be used. See Appendix I.

$$F_x = \frac{d}{dt}\frac{\partial (T_s + T_L)}{\partial u} - \omega \frac{\partial (T_s + T_L)}{\partial v}$$

$$= (M + A)\dot{u} - (M + B) v \omega \tag{29}$$

$$F_y = (M + B)\dot{v} + (M + A) u \omega \tag{30}$$

$$N = (I_b + R)\dot{\omega} + (B - A) u v \tag{31}$$

These equations give the external force and moment on the body required to move it through the fluid. The terms containing A, B, and R are the reactions of the body on the surrounding fluid.

APPENDIX III

Two Dimensional Motion of a Prolate Ellipsoid in a Frictionless Fluid

Prolate Ellipsoidal Coordinates:

$$x = c\,\eta\,\xi\ ,\quad y = r\cos\zeta\ ,\quad z = r\sin\zeta\ ,$$

$$r^2 = c^2\,(1-\xi^2)\,(\eta^2-1)\ .$$

The boundary of the prolate ellipsoid represented by the equation

$$\frac{x^2}{a^2} + \frac{y^2}{b^2} + \frac{z^2}{b^2} = 1$$

is defined by the single ellipsoidal coordinate

$$\eta = \eta_o = \frac{a}{c}\ ,\quad c^2 = a^2 - b^2\ .$$

Let the geometric center, $x = y = z = 0$, be the origin of body axes. Motion takes place in the x_o, y_o coordinate system. The motion is described as follows:

u, v	components of body velocity resolved along body axes,
ω	angular velocity of body,
U, V	components of the velocity of the fluid at a large distance from the body resolved along body axes.

The velocity potential, ϕ, for this motion is

$$\begin{aligned}\phi = {} & c\,u\,A_1\,P_1(\xi)\,Q_1(\eta) + c\,v\,A_2\,P_1^1(\xi)\,Q_1^1(\eta)\cos\zeta \\ & + c^2\,\omega\,A_3\,P_2^1(\xi)\,Q_2^1(\eta)\cos\zeta \\ & - c\,U\left[A_1\,Q_1(\eta) + P_1(\eta)\right]\,P_1(\xi) \\ & - c\,V\left[A_2\,Q_1^1(\eta) + P_1^1(\eta)\right]\,P_1^1(\xi)\cos\zeta\ .\end{aligned}$$

$$A_1 = - \frac{1}{\frac{d\, Q_1(\eta_o)}{d\,\eta}} \quad , \quad A_2 = - \frac{\eta_o}{P_1^1(\eta_o) \frac{d\, Q_1^1(\eta_o)}{d\,\eta}}$$

$$A_3 = - \frac{P_1(\eta_o)}{P_2^1(\eta_o) \frac{d\, Q_2^1(\eta_o)}{d\,\eta}}$$

The P and Q functions are Legendre's polynominals.

Define:

$$k_1 = \frac{Q_1(\eta_o)}{P_1(\eta_o)} A_1 \quad , \quad k_2 = \frac{Q_1^1(\eta_o)}{P_1^1(\eta_o)} A_2 \quad ,$$

$$k' = \frac{9}{2\eta_o^2 - 1} \frac{Q_2^1(\eta_o)}{P_2^1(\eta_o)} A_3 \quad .$$

Choose $\eta = \eta_o$, $\xi = 1$ as a reference point on the surface of the body. The pressure equation derived for moving axes in the text on page 9 is

$$\frac{p}{\rho} + \frac{1}{2} q_r^2 - \frac{\partial \phi}{\partial t} - \frac{1}{2} q_b^2 = C(t) \quad ,$$

where

$\bar{q}_b$ velocity of body,

$\bar{q} = - \bar{\nabla} \phi$ velocity of fluid,

$\bar{q}_r = \bar{q} - \bar{q}_b$ relative velocity.

The values of the quantities in the pressure equation are now given.

$$q_b^2 = u^2 + v^2 - 2\,c\,u\,\omega\,(1-\xi^2)^{\frac{1}{2}}(\eta_o^2-1)^{\frac{1}{2}}\cos\zeta + 2\,c\,v\,\omega\,\eta_o\,\xi + c^2\,\omega^2\left\{\eta_o^2\,\xi^2 + (\eta_o^2-1)(1-\xi^2)\right\}\cdot \cos^2\zeta$$

$$q_b^2{}_{\xi=1} = u^2 + (v + c\,\eta_o\,\omega)^2$$

$$q_r^2 = \frac{\eta_o^2\,(1-\xi^2)}{(\eta_o^2-\xi^2)}\,(k_1+1)^2\,(U-u)^2 + \left\{\frac{\xi^2\,(\eta_o^2-1)\cos^2\zeta}{(\eta_o^2-\xi^2)} + \sin^2\zeta\right\}(k_2+1)^2(v-V)^2 + \frac{2\,\eta_o\,\xi\,(1-\xi^2)^{\frac{1}{2}}(\eta_o^2-1)^{\frac{1}{2}}}{(\eta_o^2-\xi^2)}\,(k_1+1)\,(k_2+1)\cdot (U-u)\,(v-V)\cos\zeta + \left\{\frac{(\eta_o^2-1)\,\eta_o^2}{(\eta_o^2-\xi^2)}\left[(2\eta_o^2-1)(1-2\xi^2)\,k'-1\right]^2\cos^2\zeta + \eta_o^2\,\xi^2\left[(2\eta_o^2-1)\,k'+1\right]^2\sin^2\zeta\right\}c^2\,\omega^2 - \frac{2\eta_o^2\,(\eta_o^2-1)^{\frac{1}{2}}(1-\xi^2)^{\frac{1}{2}}}{(\eta_o^2-\xi^2)}\left[(2\eta_o^2-1)(1-2\xi^2)\,k'-1\right]\cdot (k_1+1)\,(U-u)\,c\,\omega\cos\zeta +$$

$$\left\{ \frac{-2\eta_o \xi (\eta_o^2 - 1)}{(\eta_o^2 - \xi^2)} \left[(2\eta_o^2 - 1)(1 - 2\xi^2)\, k' - 1 \right] \cos^2 \zeta \right.$$

$$\left. + 2\eta_o \xi \left[(2\eta_o^2 - 1)\, k' + 1 \right] \sin^2 \zeta \right\}$$

$$(k_2 + 1)(v - V)\, c\, \omega$$

$$q_r^2{}_{\xi=1} = \left\{ (k_2 + 1)(v - V) + \eta_o \left[(2\eta_o^2 - 1)\, k' + 1 \right] c\, \omega \right\}^2$$

$$\frac{\partial \phi}{\partial t} = c\, \dot{u}\, k_1\, \xi\, \eta_o + c\, \dot{v}\, k_2 (\eta_o^2 - 1)^{\frac{1}{2}} (1 - \xi^2)^{\frac{1}{2}} \cos \zeta$$

$$+ c\, \dot{\omega}\, k' (2\eta_o^2 - 1)(\eta_o^2 - 1)^{\frac{1}{2}} (1 - \xi^2)^{\frac{1}{2}} \eta_o\, \xi \cos \zeta$$

$$- c\, \dot{U} (k_1 + 1)\, \eta_o\, \xi$$

$$- c\, \dot{V} (k_2 + 1)(\eta_o^2 - 1)^{\frac{1}{2}} (1 - \xi^2)^{\frac{1}{2}} \cos \zeta$$

$$\frac{\partial \phi}{\partial t}_{\xi=1} = c\, \dot{u}\, k_1\, \eta_o - c\, \dot{U} (k_1 + 1)\, \eta_o$$

The relationships between the directions and magnitudes of the unit vectors $\bar{i}$, $\bar{j}$, $\bar{k}$, $\bar{\xi}$, $\bar{\eta}$, and $\bar{\zeta}$ are now given.

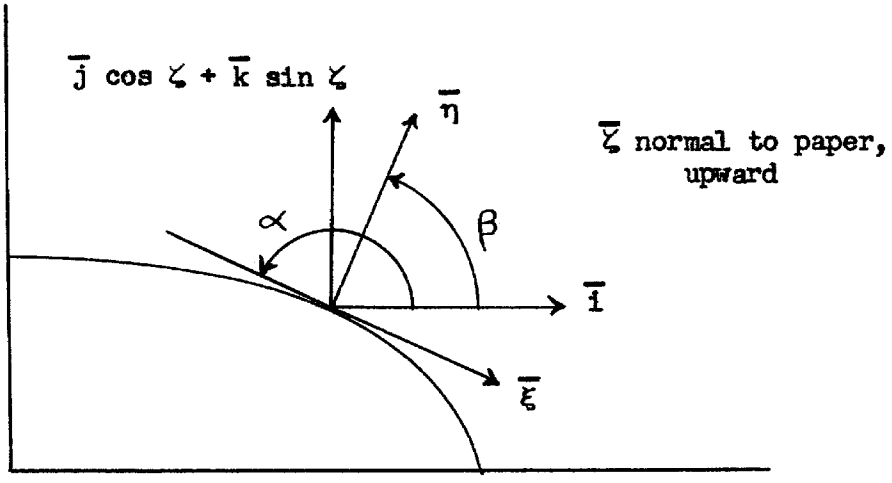

$$\tan\alpha = \frac{dr}{dx} = -\frac{b}{a}\frac{x}{(a^2 - x^2)^{\frac{1}{2}}} = -\frac{\xi\,(\eta_o^2 - 1)^{\frac{1}{2}}}{\eta_o\,(1 - \xi^2)^{\frac{1}{2}}}$$

$$\beta = \alpha - \frac{\pi}{2}$$

$$\cos\beta = \frac{\xi\,(\eta_o^2 - 1)^{\frac{1}{2}}}{(\eta_o^2 - \xi^2)^{\frac{1}{2}}}\,, \quad \sin\beta = \frac{\eta_o\,(1 - \xi^2)^{\frac{1}{2}}}{(\eta_o^2 - \xi^2)^{\frac{1}{2}}}$$

The element of surface area, dS , is given by

$$dS = c^2\,(\eta_o^2 - \xi^2)^{\frac{1}{2}}(\eta_o^2 - 1)^{\frac{1}{2}}\,d\xi\,d\zeta \quad .$$

The force and moment exerted on the body by the fluid are now given.

$$f_x = \int_S -p\cos\beta\,dS = \int_{-1}^{+1}\int_0^{2\pi} -p\,c^2\,(\eta_o^2 - 1)\,\xi\,d\xi\,d\zeta$$

$$= \frac{4}{3}\,\rho\,c^3\,\eta_o\,(\eta_o^2 - 1)\left\{(\dot{U} - \dot{u})\,k_1 + \dot{U} + (v - V)\,k_2\,\omega - V\,\omega\right\}$$

$$f_y = \frac{4}{3}\,\rho\,c^3\,\eta_o\,(\eta_o^2 - 1)\left\{(\dot{V} - \dot{v})\,k_2 + \dot{V} - (u - U)\,k_1\,\omega + U\,\omega\right\}$$

$$f_z = 0$$

$$n = \int_S \left\{ - y\, df_x + x\, df_y \right\}$$

$$= -\frac{4}{15} \rho c^5 \eta_o (\eta_o^2 - 1)(2\eta_o^2 - 1) k' \dot{\omega}$$

$$- \frac{4}{3} \rho c^3 \eta_o (\eta_o^2 - 1)(k_2 - k_1)(u - U)(v - V)$$

When the values of c and η_o are replaced by a and b and the mass, M_o, and moment of inertia, I_o, of the displaced fluid are calculated, these equations become

$$f_x = M_o \left\{ (\dot{U} - \dot{u}) k_1 + \dot{U} + (v - V) k_2 \omega - V \omega \right\} ,$$

$$f_y = M_o \left\{ (\dot{V} - \dot{v}) k_2 + \dot{V} - (u - U) k_1 \omega + U \omega \right\} ,$$

$$n = -I_o k' \dot{\omega} - M_o (k_2 - k_1)(u - U)(v - V) .$$

APPENDIX IV

Moment of Inertia of Spindle and Angular Damping Rate of Seal

The spindle was made of steel. The dimensions were 8.25 inches of .875 inch diameter and 2.75 inches of 1.0625 inch diameter. The moment of inertia of these sections is

$$I_s = \frac{1}{2} \quad m\, r^4\, a \;=\; 5.9 \times 10^{-5} \text{ lb ft sec}^2 \;.$$

Viscous laminar shear was assumed to take place in the small clearance between the spindle and tunnel wall. The equation for the damping rate is

$$B_s = \frac{F\, r}{\omega} = \frac{\mu\, (2\pi r\, a)\, (\omega\, r)}{t} \quad \frac{r}{\omega} = \frac{2\pi\, \mu\, r^3\, a}{t} \;.$$

For $r = .4375$ inch, $a = 1$ inch, $t = .001$ inch, and $\mu = 1.45 \times 10^{-7}$ lb sec in^{-2}, $B_s = .63 \times 10^{-5}$ lb ft sec.

The steady state solution for the complete system of Fig. 2 for oscillation at frequency ω is

$$\left\{ \frac{K + K_2}{K_2} - \frac{I\, \omega^2}{K_2} + \frac{j\, \omega\, B}{K_2} \right\}^{-1} = \frac{K_1 + K_2}{K_2} - \frac{I_s\, \omega^2}{K_2} + \frac{j\, B_s\, \omega}{K_2} - \frac{K_1\, \theta_2}{K_2\, \theta_1} \;.$$

At the highest frequency used, 10 cps , the quantity $\frac{I_s}{K_2}\, \omega^2$ was equal to .001 . For most runs this was negligible compared with the other terms. It was used whenever it was necessary.

The ratio of the B_s term to the I_s term was equal to .009 at 2 cps and to .002 at 10 cps. The B_s term was negligible at all times.

APENDIX V

Phase Shift in an Amplitude Modulated Wave

Since the maximum band width between the upper and lower side band frequencies is approximately two percent of the center carrier frequency, it will be assumed that any change in phase shift with frequency in the electronic equipment is proportional to frequency over this small range. This assumption is verified for the narrow pass band L-C filter in the second part of this appendix.

$E \sin \omega_c t$ — original carrier signal

$e \sin \omega_s t$ — original modulating signal

$\zeta = \zeta_o + k(\omega - \omega_c)$ — phase shift (lag)

$\left\{E + e \sin \omega_s t\right\} \sin \omega_c t$

original modulated signal

$\left\{E + e \sin (\omega_s t - \omega_s k)\right\} \sin(\omega_c t - \zeta_o)$

modulated signal after assumed phase shift

For steady state signals the phase of the carrier is delayed by the amount ζ_o. The phase of the envelope or modulating signal is delayed an amount proportional to the rate of change of phase shift. The wave form of the signal is not distorted.

Characteristics of 1000 cps L-C Filter

A single section band pass filter was used to remove noise pickup voltages from the modulated signal. It was a single section, T type

unit. Each of the two series arms was a series L-C circuit consisting of an inductor of 7.9 h and a capacitor of .0032 ufd; the shunt arm was a parallel L-C circuit consisting of an inductor of .06 h and a capacitor of .422 ufd. These values were accurate to about two percent. The calculated band width, center frequency, and load resistor were 123cps, 1000cps, and 6100 ohms.

The characteristics of the circuit were investigated analytically. When the filter is terminated in the design load resistor, the transfer constant may be expressed in the equation

$$\frac{e_o}{e_i} = \frac{1}{1 - 2\,q^2 + j\,2\,q\,(1 - q^2)} \quad ,$$

where

$$q = \frac{f_o}{\Delta f}\left\{\frac{f}{f_o} - \frac{f_o}{f}\right\} \quad ,$$

f_o = center frequency, Δf = band width.

Now:

$$\frac{d\varphi}{df} = \frac{4}{\Delta f}\,\frac{180}{\pi} = 1.863 \text{ degrees per cps at } f = f_o \quad ,$$

$$\text{Tan } \varphi = 18.30 \text{ degrees and } \frac{|e_o|}{|e_i|} = 1.0028 \text{ at } f = f_o + 10 \text{ cps.}$$

It is seen that the departure from linearity of the phase shift with frequency and the change in gain is negligibly small for the ten cps maximum oscillation frequency used.

The performance was checked experimentally. Measured band width was 134 cps and center frequency was 994 cps. The insertion loss was about two db. The measured rate of phase shift was

2.12 ± .06 degrees per cps. This measurement was made with unmodulated signals. The final calibration value for the entire circuit from pickup to load resistor was 2.17 degrees per cps. This measurement was made with the pickup unit connected to the constant amplitude drive platform motion. There was no detectable nonlinearity.

APPENDIX VI

Sample Calculations

Angular Measurement

Balance constants:

K_1 = 108 lb ft per radian,

K_2 = 185 lb ft per radian,

I_s = 5.9×10^{-5} lb ft sec^2 .

Data:

Run 41 , 5 : 1 aspect ratio , 15 fps tunnel velocity , 6 cps oscillation frequency ,

$\frac{A_2}{A_1}$ = .941 , $\alpha_1 - \alpha_2 < 0^\circ\ 18'$ (estimated).

The phase angle between the drive motion and the spindle motion could not be measured with any degree of precision for an individual run. The estimated maximum value is based on an average slope for all of the runs at a given tunnel velocity.

For these small phase angles, $\sin(\alpha_2 - \alpha_1) = (\alpha_2 - \alpha_1)$,

and the solution to Eq. (20) becomes

$$\left\{\frac{K + K_2}{K_2} - \frac{I\omega^2}{K_2}\right\}^{-1} = \frac{K_2 + K_1}{K_2} - \frac{K_1}{K_2}\frac{A_2}{A_1} - \frac{I_s\omega^2}{K_2},$$

$$\frac{\omega B}{K_2} < -\frac{K_1}{K_2}\frac{A_2}{A_1}(\alpha_2 - \alpha_1)\left\{\frac{K_2 + K_1}{K_2} - \frac{K_1}{K_2}\frac{A_2}{A_1} - \frac{I_s\omega^2}{K_2}\right\}^{-2}.$$

For Run 41:

$$\frac{K + K_2}{K_2} - \frac{I\omega^2}{K_2} = .967 \quad ,$$

which is plotted in Fig. 5 . The average slope of the phase angle was 2.6 minutes per cps oscillation frequency for the 15 fps tunnel velocity runs. This quantity was used to determine the dimensionless coefficient corresponding to the B term.

Lateral Force Measurement

Data: Run 41 , $V_o = .505$, $h = .549$, $A_t = 3$, $f = 6$,

$i_g = .99$, $\alpha_o - \alpha_i = -65.4^\circ$, $A_o = 2^\circ$.

Equation (23) is now used.

$$m\omega^2 + \ell = .197 \quad , \qquad \omega b = .431$$

These values appear on Fig. 9 and 12.

REFERENCES

(1) Milne-Thomson, L. M., Theoretical Hydrodynamics, Macmillan and Co., 1949, pp 477 - 481.

(2) Zahm, A. F., Smith, R. H., and Louden, F. A., Air Forces, Moments, and Damping on Model of Fleet Airship Shenandoah, NACA Report No. 215, Sept. 1925, Data from table XX page 23.